JAMES | Journal of Advances in Modeling Earth Systems

RESEARCH ARTICLE
10.1029/2025MS005430

Special Collection:
Integrating In Situ, Remote Sensing, And Physically Based Modeling Approaches to Understand Global Freshwater Ice Dynamics

Extending the *air2water* Model to Simulate Lake Ice Phenology, Thickness, and Composition Using Minimal Inputs

Marta Fregona[1], Matti Leppäranta[1], Joachim Jansen[1], Joonatan Ala-Könni[1], Ivan Mammarella[1], and Sebastiano Piccolroaz[2]

[1]Institute of Atmospheric and Earth System Research/Physics, Faculty of Science, University of Helsinki, Helsinki, Finland, [2]Department of Civil, Environmental and Mechanical Engineering, University of Trento, Trento, Italy

Key Points:

- New ice module added to *air2water* simulates ice timing and thickness using only air temperature and precipitation
- Strong performance on Finnish lakes with root mean square errors 1°C for lake surface water temperature and about 10 cm for ice thickness
- Accurate ice thickness prediction with minimal input data highlights the model's efficiency for climate and ecological studies

Supporting Information:

Supporting Information may be found in the online version of this article.

Correspondence to:

S. Piccolroaz and M. Fregona,
s.piccolroaz@unitn.it;
marta.fregona@helsinki.fi

Citation:

Fregona, M., Leppäranta, M., Jansen, J., Ala-Könni, J., Mammarella, I., & Piccolroaz, S. (2026). Extending the *air2water* model to simulate lake ice phenology, thickness, and composition using minimal inputs. *Journal of Advances in Modeling Earth Systems*, *18*, e2025MS005430. https://doi.org/10.1029/2025MS005430

Received 18 AUG 2025
Accepted 23 JAN 2026

Author Contributions:

Conceptualization: Sebastiano Piccolroaz
Data curation: Marta Fregona, Sebastiano Piccolroaz

Abstract Ice cover in seasonally frozen lakes plays a crucial role in ecosystem dynamics and human activities, while also serving as a sensitive indicator of climate change. Accurate yet efficient modeling of lake ice timing and thickness is therefore increasingly important. This study presents a new ice module integrated into the existing *air2water* model, a hybrid physics-based/statistical model originally developed to predict lake surface water temperature (LSWT) using air temperature as its sole input. The extended model simulates ice cover dynamics, distinguishing between black ice (formed by direct lake water freezing) and white ice (from accumulated snow submerged and frozen over black ice). The extension preserves the original framework's key advantages: minimal input requirements (air temperature and precipitation), low parametrization (8–11 parameters), and physically based governing equations. Calibration was performed using an automatic optimization algorithm with a multi-objective performance metric combining LSWT and ice thickness Nash-Sutcliffe efficiency indices (NSEs). Evaluation employed long time series (1960–2023) of LSWT and ice thickness data from three Finnish lakes spanning different climatic conditions. When calibrated with equal weighting of LSWT and ice thickness NSEs, the model demonstrated robust performance across all lakes, with daily LSWT root mean square errors (RMSEs) near 1°C and ice thickness RMSEs of about 10 cm. Notably, consistent ice thickness predictions were achieved even when calibration relied solely on LSWT data. LSWT simulations also improved relative to the original model. These results show that the extended *air2water* model offers a competitive and data-efficient alternative to more complex lake ice models.

Plain Language Summary Most lakes in mid- and high-latitude regions freeze during winter. Understanding ice formation and melting is important for climate studies, ecosystems, and human activities. Ice timing and thickness are sensitive indicators of climate change. Ice cover also affects aquatic life by influencing oxygen levels, greenhouse gas release, and biodiversity, and it impacts human activities such as winter transportation, fishing, and recreation. This study presents a simple yet robust model that predicts lake surface water temperature and ice cover dynamics, including timing, thickness, and two types of ice: black ice (from direct freezing of lake water) and white ice (from accumulated snow submerged and frozen over black ice). The model requires only air temperature and precipitation as inputs. We tested the model on three Finnish lakes using data from 1960 to 2023. Results showed the model predicts daily water temperatures within about 1°C and ice thickness within about 10 cm. This strong performance is notable given the model's simplicity and is comparable to more complex approaches. Overall, the model offers an effective and user-friendly tool for simulating lake ice, helping researchers and policymakers study lake environments and climate change impacts without relying on complex or data-heavy models.

1. Introduction

Most of the world's lakes are located above a latitude of 45°N in north-temperate, boreal and Arctic regions, where they are typically subject to seasonal ice cover (Verpoorter et al., 2014; Yang et al., 2021). However, growing evidence indicates that these lakes are experiencing a marked and accelerating decline in ice cover due to climate change, particularly over the past 25 years (Hampton et al., 2024; He et al., 2025). This trend is expected to have widespread ecological and societal implications, prompting sustained interest among limnologists in understanding the dynamics of lake ice and its broader impacts, as well as in advancing integrated approaches for its modeling, monitoring, and remote sensing (Culpepper et al., 2025; Hampton et al., 2024). Indeed, lake ice plays a fundamental role in regulating key physical and chemical processes. Changes in its duration and extent influence

Formal analysis: Marta Fregona, Sebastiano Piccolroaz
Investigation: Marta Fregona, Sebastiano Piccolroaz
Methodology: Marta Fregona, Matti Leppäranta, Ivan Mammarella, Sebastiano Piccolroaz
Software: Marta Fregona, Sebastiano Piccolroaz
Supervision: Matti Leppäranta, Ivan Mammarella, Sebastiano Piccolroaz
Visualization: Marta Fregona, Sebastiano Piccolroaz
Writing – original draft: Marta Fregona, Sebastiano Piccolroaz
Writing – review & editing: Matti Leppäranta, Joachim Jansen, Joonatan Ala-Könni, Ivan Mammarella

thermal structure, mixing regimes, oxygen exchange with the atmosphere, and light penetration into the water column (Flaim et al., 2020; W. Huang et al., 2021; Jansen et al., 2021; Leppäranta, 2015). These shifts affect lake ecosystems at multiple levels, altering biogeochemical cycles, species interactions, and overall productivity (Imrit & Sharma, 2021; Sharma et al., 2020; Woolway et al., 2021).

Beyond its ecological significance, lake ice has historically shaped human activity in cold regions. In the past, it was harvested to store perishable goods and facilitated the development of specialized fishing methods. Even today, frozen lakes support winter transportation and serve as vital corridors for remote communities (Beyene & Jain, 2020; Leppäranta, 2015). They also provide a setting for traditional and recreational activities such as ice fishing, skiing, long-distance skating, and ice sailing (Heinilä et al., 2021; Kirillin et al., 2012). In recent decades, however, lake ice has become increasingly thin, less stable and persists for shorter durations due to rising temperatures (Imrit & Sharma, 2021; Sharma et al., 2024; Weyhenmeyer et al., 2010; Woolway et al., 2022). These changes pose significant challenges: ice roads open later or become impassable, winter festivals are canceled, and the risk of accidents on weakened ice increases (Hampton et al., 2024; Knoll et al., 2019). As the reliability of ice cover declines, so too does the safety and cultural continuity of many northern communities, underscoring the urgent need for improved monitoring and modeling of lake ice dynamics (Sharma et al., 2019; L. Huang et al., 2022).

Lake ice exists in two primary forms, black ice and white ice, each with distinct physical characteristics that influence stability and strength. Black ice forms when lake water directly freezes, creating a clear, dense, and strong layer. In contrast, white ice develops when the snow layer on top of the ice becomes saturated with water, which can occur either when the weight of the snow overcomes the buoyancy of the ice, or as a result of surface melting and rainfall. Once saturated, the snow refreezes, forming a dense, opaque ice layer (Leppäranta, 2015). Due to this formation process, white ice is more porous and less dense, making it weaker than black ice. It also has higher reflectance and light attenuation, resulting in both a lower bearing capacity and reduced sunlight penetration. As climate conditions warm, these differences in ice quality (IQ) become increasingly important. Warmer temperatures have been linked to thinner layers of black ice, while white ice tends to become more prevalent and, in some cases, the dominant component of the ice layer, especially toward the end of the ice-covered season (Culpepper et al., 2024). This shift in composition results in ice that is both structurally weaker and reduces light transmission to the water column with possible implications for under-ice ecological processes. For example, white ice inhibits the development of radiatively-driven convection (Smith et al., 2025), which in turn could impede suspension of diatoms and decrease the intensity of under-ice algal blooms (Kelley, 1997). With continued trends of reduced maximum ice thickness, shorter periods of ice cover, and increased dominance of weaker white ice (L. Huang et al., 2022; Weyhenmeyer et al., 2022), concerns are growing about the implications for human safety as well as the broader impacts on aquatic ecosystems.

In light of the changes discussed above, the ability to reconstruct past trends and predict future dynamics in lakes is increasingly important. However, ice monitoring remains sporadic, with long term records available only in a few regions and for a relatively small number of lakes. This underscores the need for reliable models capable of accurately simulating ice thickness, IQ, ice cover duration, and snow cover on ice to reconstruct past variability and project future changes. Models for ice simulation can be developed as standalone systems (Duguay et al., 2003; Launiainen & Cheng, 1998), but incorporating them as modules into lake temperature models provides a more comprehensive and efficient approach since ice and water temperature in lakes are tightly coupled (Zhou et al., 2024). Over time, various models with different levels of complexity have been developed to represent thermal dynamics in lakes, some of which include a lake ice module (see Piccolroaz et al. (2024) for a review). While many of these models simulate ice thickness, ice cover duration, and thermal dynamics, it is important to note that only a subset of these ice models/modules also simulate IQ (black and white ice distinction), a critical factor for assessing the structural integrity and safety of lake ice, which can vary significantly based on environmental conditions. Models simulating ice dynamics in lakes span from simple regressions (Ashton, 1980) to complex process-based models (Cheng et al., 2003; Leppäranta, 1983; Yang et al., 2012). Traditional regression models are generally easy to use and typically require little input information, making them convenient when data are limited (Livingstone & Lotter, 1998; McCombie, 1959; Sharma et al., 2008). In addition to these models, machine learning approaches have gained attention for simulating lake thermal dynamics and ice cover (Hazem & Cary, 2025; He et al., 2025). However, they typically require large data sets for training and optimization. While they can outperform traditional regression models in capturing complex, nonlinear relationships, their reliance on extensive observational data can be a limitation. In general, the performance of both types of

models is highly dependent on the quality of the available data and their reliability may be questionable when applied to input variables that exceed the range used for model calibration, such as in climate change studies (Piccolroaz & Toffolon, 2018; Piccolroaz et al., 2024) or when analyzing extreme events (Jankowski et al., 2006; Shinohara et al., 2023). On the other hand, deterministic, physically based models are able to return a more detailed representation of lake thermal dynamics but depend on extensive meteorological data sets, which could not be available or accurate enough (Gaudard et al., 2019; Martynov et al., 2010; Perroud et al., 2009; Thiery et al., 2014). These models require the formulation of fundamental principles and the establishment of relationships between variables, based on either empirical or theoretical laws. In cases where scientific knowledge is limited, deterministic models often rely on simplifying assumptions, which inevitably constrain the range of simulated processes: a clear example is the minimal physical model for freeze-up timing proposed by Toffolon et al. (2021).

Between purely regression-based and deterministic physically based models, another category can be identified: hybrid models. Hybrid models are those that integrate data-driven techniques (statistical or machine learning methods) with processed-based approaches. The *air2water* model proposed by Piccolroaz et al. (2013) is an example of a hybrid model. It is a 0.5D model (i.e., a box model, see Piccolroaz et al. (2024)) for simulating lake surface water temperature (LSWT), representing a time-varying, well-mixed surface layer that captures stratification and vertical mixing without resolving the full depth profile. It combines the simplicity and efficiency of statistical models with the robust performance of more complex deterministic models, leveraging its foundation in physical principles. The purpose of this work is to extend the *air2water* model by introducing an additional module to simulate ice occurrence, timing, thickness, and quality. The ice module was developed based on a solid physical foundation, but preserving the model's simplicity (i.e., a limited number of equations) and parsimony (i.e., a small number of parameters and input variables). To evaluate its performance, the extended model was tested on three Finnish lakes with different climatic conditions, for which LSWT, ice thickness, and IQ data are available.

2. Materials and Methods

2.1. The *air2water* Model

The *air2water* model, described in Piccolroaz et al. (2013), is a hybrid physics-based/statistical model that simulates LSWT, here representing water temperature in the epilimnion, by using air temperature as the only forcing factor. The model was developed to capture the complexity of the heat budget governing lake thermal dynamics, while avoiding reliance on numerous hydrometeorological inputs that are often unavailable (Piccolroaz et al., 2013). In its original formulation, the model identifies the start and end of the ice season based solely on LSWT data, using a fixed threshold (e.g., 0°C) to determine freezing and thawing conditions.

The model is based on a simplified representation of the surface layer heat budget, evaluated on a daily timescale. The volume-integrated heat conservation law is expressed through the following equation:

$$\rho_{water} c_p V \frac{dT_{water}}{dt} = H_{net} A, \tag{1}$$

where ρ_{water} is the water density, c_p is the specific heat at constant pressure, V is the volume of the surface well-mixed layer (whose depth varies dynamically with thermal stratification), T_{water} is LSWT, t is time, and A is the surface area of the lake. The H_{net} term represents the net heat flux into the surface layer (positive downwards), resulting from the various heat fluxes entering and leaving the upper lake volume, under the assumption that the dominant exchanges occur at the interfaces between the lake and the atmosphere. In the model, the net heat flux term is linearized and parameterized to depend only on time, air temperature (T_{air}), and LSWT (for more details, see Piccolroaz et al. (2013) and Piccolroaz (2016)). This leads to the introduction of parameters $\hat{a}_1$ to $\hat{a}_6$, allowing Equation 1 to be rewritten as:

$$\frac{dT_{water}}{dt} = \frac{1}{\rho_{water} c_p D} H_{net} = \frac{1}{\rho_{water} c_p D}\left(\hat{a}_1 + \hat{a}_2 T_{air} - \hat{a}_3 T_{water} + \hat{a}_5 \cos\left[2\pi\left(\frac{t}{t_y} - \hat{a}_6\right)\right]\right), \tag{2}$$

where t_y is the duration of the year expressed in days, and $D = V/A$ is the depth of the well-mixed surface layer. Instead of using D directly, the model employs the normalized depth $\delta = D/D_r$, where D_r is the maximum mixed layer thickness (approximately the mean depth of the lake). The normalized depth δ is empirically parameterized as a function of the vertical water temperature gradient. To capture seasonal variations, δ is parameterized differently during periods of normal and inverse stratification, according to the following relationships:

$$\begin{aligned} \delta &= \exp\left(\frac{T_r - T_{water}}{a_4}\right) T_{water} \geq T_r \\ \delta &= \exp\left(\frac{T_{water} - T_r}{a_7}\right) + \exp\left(\frac{T_f - T_{water}}{a_8}\right) T_{water} < T_r, \end{aligned} \tag{3}$$

where T_r is a reference value of temperature representative of deep-water temperature that can be chosen based on the lake thermal regime (Piccolroaz et al., 2013) (i.e., $T_r = 4$ °C for dimictic lakes), T_f is the freezing temperature (i.e., 0°C for freshwater), and a_4 and a_7 are exponential decay parameters for the warming and cooling periods, respectively. Finally, a_8 is an exponential decay parameter introduced to represent the insulating effect of ice cover, causing a fictitious increase in δ as T_{water} approaches the freezing temperature T_f. This served as a rudimentary first attempt to incorporate ice cover effects into the model (Piccolroaz et al., 2013).

By implementing the definition of δ in Equation 2, the final equation for LSWT becomes:

$$\frac{dT_{water}}{dt} = \frac{1}{\delta}\left\{a_1 + a_2 T_{air} - a_3 T_{water} + a_5 cos\left[2\pi\left(\frac{t}{t_y} - a_6\right)\right]\right\}, \tag{4}$$

and together with the expressions in Equation 3 represents the complete configuration of the *air2water* model. In Equation 4, the parameters a_i with $i = 1, \ldots, 3, 5, 6$ are related to the corresponding parameters $\hat{a}_i$ through the following relationship:

$$a_i = \frac{\hat{a}_i}{\rho_{water} c_p D_r}. \tag{5}$$

The meaning of the model parameters in Equations 3 and 4 is summarized in Table S2 in Supporting Information S1 (for more details see Toffolon et al. (2014)).

2.2. Ice Module

The ice module was developed as an extension of the *air2water* model, with the goal of preserving its simplicity, parsimony, and physical grounding, while maintaining strong performance and ensuring comparability with other deterministic models. It adopts a three-layer scheme to simulate ice thickness and snow depth, distinguishing between black ice, white ice, and the snow layer. Prior to freezing, white ice originates as slush, a mixture formed when liquid water infiltrates the lower part of the snow layer and saturates its pores. This infiltrated water may derive from lake flooding, snowmelt, or liquid precipitation. Compared to the original *air2water* model, the only additional input variables required are precipitation and an approximate value for the lake's mean depth. The ice module has distinct parameterizations for the ice growth and ice melt phases, as described in the next sections and schematized in the flowcharts in Figures S1–S5 in Supporting Information S1. We refer the reader to Table S1 in Supporting Information S1 for the list of symbols, their definitions and physical units.

2.2.1. Equation for Ice Growth Phase

The description of the ice growth phase is based on the heat conduction equation and follows Stefan's Law (Stefan, 1889). Stefan's classical formulation assumes a single ice layer and introduces the following simplifications: (i) vertical temperature gradients dominate over horizontal ones, allowing for a one-dimensional vertical model; (ii) thermal inertia is negligible, implying that the system reaches an equilibrium temperature distribution instantaneously (quasi-steady-state); (iii) no internal heat sources are present, resulting in a linear temperature profile within the ice; and (iv) the ice/air and ice/water interfaces define the upper and lower boundaries, respectively, with convective heat fluxes to the atmosphere being neglected (Leppäranta, 1993).

The heat released during ice formation at the ice/water interface is assumed to be entirely conducted through the ice and lost to the atmosphere via the ice/air interface. Therefore, the rate of ice growth is determined by enforcing the continuity of heat fluxes at the two boundaries, according to:

$$\rho_i L_f \frac{dh_i}{dt} = k_i \frac{T_f - T_{ia}}{h_i}, \tag{6}$$

where ρ_i is the ice density, L_f is the latent heat of freezing, T_{ia} is the temperature at the ice/atmosphere boundary, k_i is the thermal conductivity of ice, and h_i is the ice thickness. Here, the subscript i refers to ice in general and should not be confused with the subscript i in the model parameters (a_i), which denotes the parameter index.

Since direct measurements of T_{ia} are often unavailable, whereas air temperature at a certain height above the surface is commonly recorded, Stefan's Law in Equation 6 is usually coupled with the atmosphere by expressing T_{ia} as a function of T_{air} (e.g., Leppäranta (1993)). The coupling is modeled by equating the convective heat flux from the ice surface to the atmosphere with the conductive heat flux through the ice, driven by the temperature difference between the ice/air and ice/water interfaces (Barnes, 1928; Zhaka et al., 2021):

$$c_a (T_{ia} - T_{air}) = k_i \frac{T_f - T_{ia}}{h_i}, \tag{7}$$

where c_a is a semi-empirical parameter that represents the air convective heat transfer coefficient (Ashton, 1989). This equality allows deriving an expression for T_{ia} as a function of T_{air}, which can be substituted into Equation 6, yielding an ice growth equation that incorporates ice–atmosphere coupling:

$$\rho_i L_f \frac{dh_i}{dt} = \frac{T_f - T_{air}}{h_i/k_i + 1/c_a} = \frac{a_9 - T_{air}}{h_i/k_i + 1/a_{10}}. \tag{8}$$

In this formulation, two parameters are introduced. Parameter a_9 compensates for possible discrepancies arising from air temperature measurements, which are typically taken at weather stations located some distance from the lake and a few meters above the ground. It also accounts for potential biases when using reanalysis data sets, as well as deviations of the freezing temperature T_f from the standard 0°C value for freshwater. Its a priori range is set between −10 and 10°C, broad enough to encompass expected deviations. Parameter a_{10} represents the convective heat transfer coefficient c_a, which varies substantially (typically between 10 and 25 W m^{-2} K^{-1}; Ashton (1989)). Both parameters are physically meaningful and defined within realistic bounds.

The equation describing black-ice growth is derived from Equation 8, with additional terms accounting for the insulating effects of the overlying white-ice and snow layers. The same approach used to express T_{ia} as a function of T_{air} (see Equation 7) is applied to determine the temperatures at the black-ice/white-ice (T_{bw}), white-ice/snow (T_{ws}), and snow/atmosphere (T_{sa}) interfaces (see Figure 1). By enforcing continuity of heat flux at each interface, and substituting the freezing temperature T_f and convective heat transfer coefficient c_a with parameters a_9 and a_{10}, the model incorporates the insulating effects of these layers, yielding the equation used to simulate black-ice growth (see Text S1 in Supporting Information S1 for the derivation):

$$\frac{dh_b}{dt} = \frac{1}{\rho_b L_f} \left(\frac{a_9 - T_{air}}{h_b/k_b + h_w/k_w + h_s/k_s + 1/a_{10}} \right), \tag{9}$$

where ρ_b is the black-ice density, h_b, h_w, and h_s are the black-ice, white-ice, and snow thicknesses, respectively, and k_b, k_w, and k_s are the corresponding heat conductivities. In the model, the heat conductivities of black ice and white ice are assumed to be equal and set to $k_b = k_w = k_i = 2$ W m^{-1} °C^{-1}, due to their low variability (less than 10%; Cheng, 2017; Pringle et al., 2006). Similarly, the densities of both ice types are set to a constant value of $\rho_i = 917$ kg m^{-3} (Zhaka et al., 2021). Finally, the thermal conductivity of snow is assumed constant at 0.3 W m^{-1} °C^{-1} (Yen, 1981) and the latent heat of fusion (L_f) is taken as 3.34×10^5 J kg^{-1} (Gaudard et al., 2019).

The equation describing white-ice growth is derived by simplifying the black-ice growth equation, considering only the insulating effect of the snow layer above the white ice:

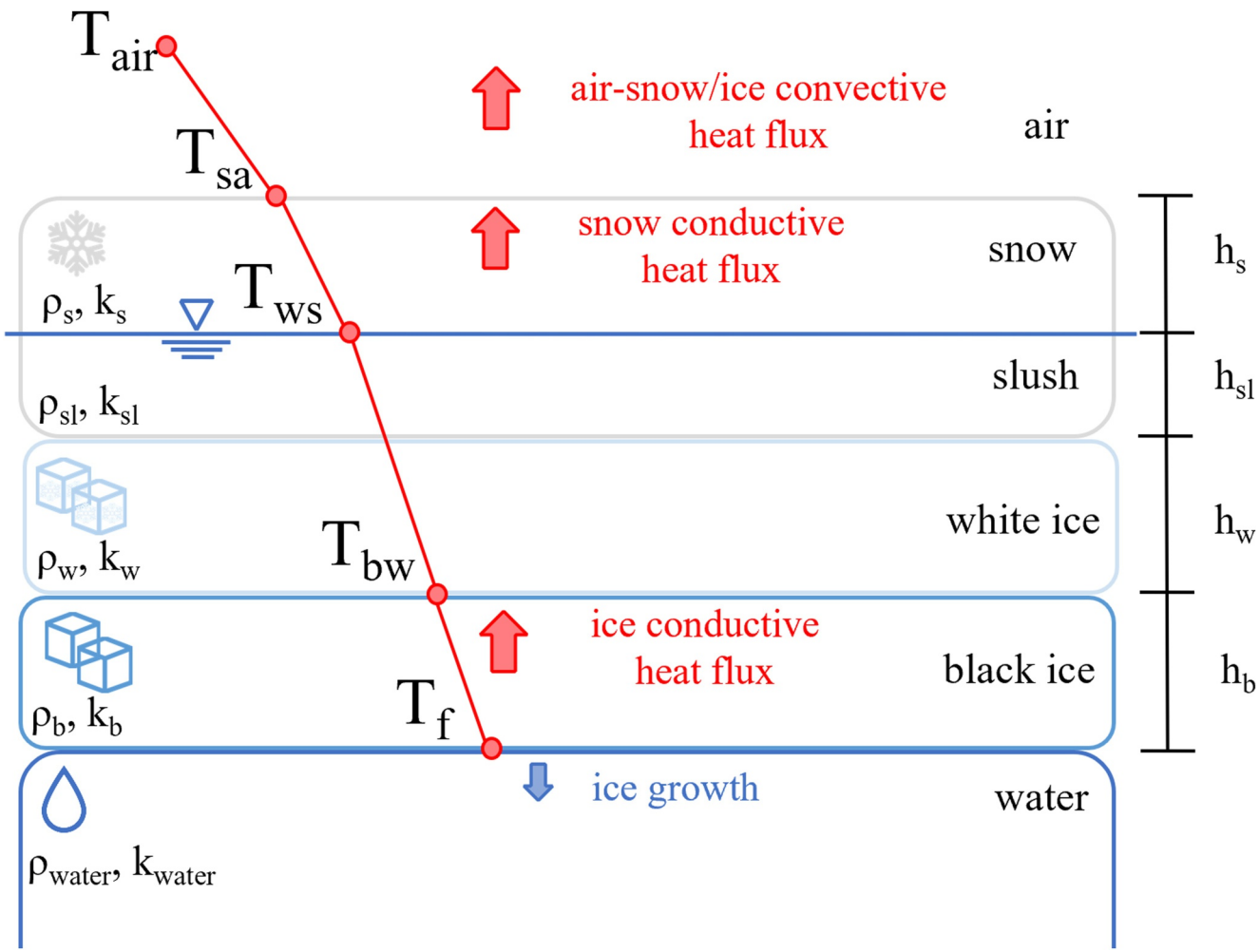

Figure 1. Schematic of the layers considered in the ice module. For each layer (water, black-ice, slush/white-ice, and snow), the corresponding density (ρ), thermal conductivity (k), and thickness (h) are indicated. T_f represents the freezing temperature (0°C for freshwater), T_{air} is the air temperature, and T_{bw}, T_{ws}, and T_{sa} are the temperatures at the white black-ice/white-ice, white-ice/snow and snow/air interfaces, respectively.

$$\frac{dh_w}{dt} = \frac{1}{L_f \rho_i e} \frac{(a_9 - T_{air})}{(h_s/k_s + 1/a_{10})}, \tag{10}$$

where the snow porosity (e) accounts for the fact that only the liquid fraction of the slush needs to freeze (Leppäranta & Kosloff, 2000). Snow porosity is estimated by considering the snow layer as a mixture of ice and air. Applying mass balance gives: $\rho_s h_s = \rho_i h_s (1 - e) + \rho_{air} h_s e$, where ρ_s is the snow density (assumed 300 kg m^{-3}, Zhaka et al., 2021), ρ_i the ice density, and ρ_{air} the air density. Neglecting the air mass contribution due to its low density, porosity simplifies to $e = 1 - (\rho_s/\rho_i)$.

Alternating layers of white ice and slush often form because new snow can accumulate on slush before it fully freezes (Saloranta, 2000). The model does not explicitly simulate this stratification; instead, it represents white ice as a single layer adjacent to the black ice, while all remaining or newly formed slush is combined into a single overlying layer.

2.2.2. Equation for Ice Melting Phase

When the net heat flux exchanged at the air/ice interface (H_{net}) is positive, the rate of ice thickness decrease due to melting is given by:

$$\frac{dh_L}{dt} = -\frac{H_{net}}{\rho_L L_f} = -\frac{a_{11} D_r \rho_{water} c_p}{\rho_L L_f}\left\{a_1 + a_2 T_{air} + a_5 cos\left[2\pi\left(\frac{t}{t_y} - a_6\right)\right]\right\}, \quad (11)$$

with h_L and ρ_L denoting the thickness and density of the uppermost layer of the ice column (black ice, white ice, or snow). In this formulation, the ice melting equation mirrors the *air2water* LSWT model presented in Equation 2, with H_{net} parameterized through the same coefficients $\{\hat{a}_i\}$ but with $T_{water} = 0$°C since the surface ice layer is assumed to remain at the freezing point during the melting phase. Each $\hat{a}_i$ is replaced by the corresponding a_i using Equation 5, so that the same model parameters are shared between the original *air2water* model and the ice module. In this substitution, the lake mean depth (D_r) appears explicitly as the only lake-specific constant required by the model. Additionally, a dimensionless parameter a_{11} is introduced to account for potential differences in heat flux parameterization between ice-covered and ice-free conditions (e.g., changes in albedo and turbulent exchange coefficients). The parameter's range is constrained between 0.5 and 1.5, reflecting that only minor adjustments are expected since the physical processes governing the heat exchange remain the same.

2.2.3. Structure of the Ice Module

The ice module is activated whenever the modeled LSWT, T_{water}, falls below the freezing point ($T_f = 0$ °C) or when the simulated ice thickness (black ice, h_b) exceeds zero. The flowcharts summarizing the structure and logic of the ice module are provided in Figures S1–S5 in Supporting Information S1.

As a first step, the water temperature is set to the freezing point T_f. Precipitation, provided as input, is then classified as rainfall or snowfall based on an air temperature threshold: if $T_{air} > a_9 + a_{12}$ precipitation falls as rainfall; otherwise, it is treated as snowfall. The parameter a_{12}, which ranges from 0 to 10°C to accommodate potentially low values of a_9, adjusts the phase-change threshold to account for snowfall occurring at air temperatures slightly above the freezing point. Precipitation is evaluated at the current and subsequent time steps to compute mean snowfall and rainfall rates. Snow depth is then updated accordingly, accounting also for evaporation losses, which are assumed constant at $E = 0.001$ m day^{-1} (Jordan, 1991).

The contributions of rainfall and flooding to the slush layer are then evaluated. The increase in slush thickness due to rainfall ($\Delta h_{sl,Rf}$) is calculated by dividing the mean rainfall depth by the snow porosity e. The increase in slush thickness from flooding $\Delta h_{sl,f}$ occurs when the weight of the overlying snow layer exceeds the buoyant force exerted by the underlying ice and slush layers, resulting in their partial submersion:

$$\rho_s h_s > \left(\rho_{water} - \rho_i\right) h_b + \left(\rho_{water} - \rho_i\right) h_w + \left(\rho_{water} - \rho_{sl}\right) h_{sl}, \quad (12)$$

with ρ_{sl} the density of slush (defined as $\rho_{sl} = \rho_{water} + \rho_s\left(1 - \rho_{water}/\rho_i\right)$) and h_{sl} the thickness of the slush layer already formed. According to mass conservation, the reduction in snow mass due to flooding is equal to the increase in the buoyant weight of the ice and slush layers that become submerged. This balance is expressed as:

$$\rho_s h_s - \rho_s \Delta h_{sl,f} = \left(\rho_{water} - \rho_i\right)\left(h_b + h_w\right) + \left(\rho_{water} - \rho_{sl}\right) h_{sl} + \left(\rho_{water} - \rho_{sl}\right)\Delta h_{sl,f}. \quad (13)$$

From Equation 13 it is possible to derive the expression for the slush thickness increase due to flooding ($\Delta h_{sl,f}$):

$$\Delta h_{sl,f} = \frac{\rho_s h_s - \left(\rho_{water} - \rho_i\right)\left(h_b + h_w\right) + \left(\rho_{water} - \rho_{sl}\right) h_{sl}}{\rho_s + \rho_{water} - \rho_{sl}}. \quad (14)$$

Finally, slush thickness is updated considering both rainfall and flooding contributions.

After these preliminary steps, the ice module simulates the ice growth and melting phases separately. The model enters the ice growth phase when $T_{air} < \left(T_f + a_9\right)$. Similarly to Equation 8, the parameter a_9 is introduced to compensate for potential biases in the air temperature input, whether from in situ measurements or reanalysis data sets. In the presence of slush available for freezing, the increase in white-ice thickness (Δh_w) is calculated using Equation 10. Subsequently, the ratio $h_{sl}/\Delta h_w$ is evaluated to determine how much of the slush layer has frozen into white ice. If $h_{sl}/\Delta h_w > 1$, a residual slush layer remains, and no black-ice growth occurs. Only when slush is

fully depleted, that is, $h_{sl}/\Delta h_w < 1$, the growth of black ice is triggered according to Equation 8. In this case, the excess energy, still available after freezing the entire layer of slush, contributes to the increase of the existing black-ice thickness (see flowchart in Figure S4 in Supporting Information S1).

Otherwise, if $T_{air} \geq (T_f + a_9)$ and ice is present, the model switches to the melting phase. First, the heat flux is computed using the *air2water* parameterization defined in Equation 11. Then, within the melting phase, the model distinguishes among two structural configurations, each handled separately. When the mean surface heat flux is negative (i.e., heat is lost from the lake to the atmosphere), the thicknesses of black ice and white ice are held constant at their current values. This condition prevents the melting equation from being inappropriately applied during periods that may still favor ice growth. Fluctuations in atmospheric conditions can lead to a negative mean flux even when air temperatures are above freezing. Rather than representing a physical mechanism observed in natural ice covers, this pragmatic condition is introduced as a modeling artifact to avoid nonphysical growth. In contrast, in case of a positive mean heat flux, and the presence of ice cover, the melting equation Equation 11 is applied sequentially to the layers of the system, starting from the snow. If the snow layer completely melts, the model assumes no snow remains for new slush formation. If a snow layer remains, the melted snow contributes to an increase in slush thickness ($\Delta h_{sl,m}$). Subsequently, the melting proceeds in order through the white-ice and black-ice layers, with each successive layer melting only after the previous one has been fully depleted. The model does not account for melting at the bottom boundary (ice/water interface), assuming that the water body remains thermally passive beneath the ice cover.

2.3. Numerical Solution and Model Calibration

The ordinary differential Equations 4 and 9 are solved numerically using the Crank–Nicolson scheme (see Text S2 in Supporting Information S1). To enable the solution of these equations, the input time series of daily air temperature and precipitation must be continuous, with any gaps appropriately filled. However, time series for LSWT, ice thickness, and IQ used for calibration do not require to be continuous.

In this work, model calibration was performed in two sequential steps. The first step involved calibrating the original *air2water* model using its six-parameter version, selected as a balanced compromise between the simplistic four-parameter version and the eight-parameter version, which includes a rudimentary parameterization of ice phenology (Piccolroaz et al., 2013). The purpose of this initial calibration was to constrain the parameters governing surface heat fluxes and stratification, namely a_1 through a_6, which are also used in the ice module's melting equation, with the exception of a_4. For the first calibration step, parameter ranges were defined a priori based on physically plausible values derived from empirical relationships between model parameters and lake morphometric characteristics, as described in Toffolon et al. (2014) and Piccolroaz (2016).

In the second calibration step, the full model including the ice module was calibrated. To improve parameter identifiability and reduce the risk of overparameterization, narrower ranges were adopted for the flux-related parameters a_1 to a_6, based on the optimal values obtained from the first calibration step. Specifically, for a_1 and a_4 to a_6, the new bounds were defined as ±80% of the previously calibrated value. For a_2 and a_3, which can vary over several orders of magnitude and are more sensitive to scale, the same scaling was applied in logarithmic space. The ranges for parameters a_9 to a_{12} (ice module related parameters) were set based on realistic values of the variables they are replacing (see Section 2.2), with a_{10} ranging from 0 to 35 W m^{-2} K^{-1} to allow for flexibility beyond the typical physical range.

Model calibration was carried out using a Monte Carlo–based optimization framework, in which a large ensemble of parameter sets was sampled and assessed through the Nash–Sutcliffe Efficiency (NSE) index (Nash & Sutcliffe, 1970). The optimization was performed using the Particle Swarm Optimization algorithm (Kennedy & Eberhart, 1995), previously applied in the *air2water* model. In our simulations, we used 2,000 runs and 2,000 particles, a configuration sufficiently large to guarantee stable and well-converged parameter estimates. A multiobjective formulation was adopted, combining the NSE for LSWT (NSE_{LSWT}) and the NSE for total ice thickness ($NSE_{h_{ice}}$) into a single objective function as follows:

$$NSE_{tot} = \beta NSE_{LSWT} + (1 - \beta) NSE_{h_{ice}}, \tag{15}$$

where β is a user-defined weight in the range [0,1], allowing the calibration to prioritize LSWT only ($\beta = 1$), ice thickness only ($\beta = 0$), or any weighted combination of the two metrics. The case $\beta = 1$ is particularly relevant, as ice thickness data are often unavailable or sparse, whereas LSWT observations are generally more accessible.

We also implemented the possibility to calibrate the model using IQ data (black and white-ice thickness) when available. For this purpose, the NSE was modified as follows:

$$NSE_{ice-quality} = \beta NSE_{LSWT} + (1-\beta)\frac{NSE_{h_b} + NSE_{h_w}}{2}, \quad (16)$$

where NSE_{h_b} and NSE_{h_w} are the NSE indices for black-ice and white-ice thickness, respectively.

Six different calibration configurations were considered: (a) the original *air2water* model with six parameters (*air2water* 6 par); (b) *air2water* with the ice module, calibrated using only LSWT ($\beta = 1$); (c) *air2water* with the ice module, calibrated using both LSWT and total ice thickness weighted equally ($\beta = 0.5$); (d) *air2water* with the ice module, calibrated using LSWT and black/white-ice thickness weighted equally ($\beta = 0.5$ and IQ); (e) *air2water* with the ice module, calibrated using only total ice thickness ($\beta = 0$); and (f) *air2water* with the ice module, calibrated using only black/white-ice thickness ($\beta = 0$ and IQ). For each configuration, 10 independent runs were performed to evaluate model stability and convergence.

Finally, to provide a more direct measure of model error magnitude, the root mean square errors (RMSE) were calculated in post-processing for daily LSWT and for total ice, black-ice, and white-ice thicknesses. Additionally, mean errors (MEs) were calculated for ice-on and ice-off dates. To ensure consistency across all model configurations, including the original *air2water* 6-parameter version that does not simulate ice thickness, we applied a uniform definition for ice phenology. Ice-on was defined as the first day after the previous ice-off when LSWT drops to 0°C after being above 0°C for at least two consecutive months. Ice-off was defined as the first day, after the previous ice-on date, when LSWT rises above 0°C and remains above 0°C for at least two consecutive months. This LSWT-based approach differs from the definitions used for the observed data, where ice-on corresponds to the first day after the previous ice-off when the lake is fully ice-covered, and ice-off is defined as the first fully ice-free day following ice-on. Despite this discrepancy and the model's local application without accounting for spatial variability, this approximation remains reasonably acceptable as a first estimate of ice-cover phenology.

2.4. Study Sites

The model was tested on three Finnish lakes located in distinct climatic regions characterized by varying snow cover durations (Finnish Meteorological Institute, 2025): Lake Kilpisjärvi in Northern Finland (arctic tundra), Lake Kallavesi in Central Finland (boreal), and Lake Pyhäjärvi in Eura, Southern Finland (boreal). The geographical locations of the lakes are shown in Figure 2, overlaid on a background map indicating the typical number of snow days.

Lake Kilpisjärvi is an oligotrophic lake in the Arctic tundra, situated at 473 m above sea level. It has a surface area of 37.1 km^2 and mean and maximum depths of 19.5 and 57 m, respectively (Leppäranta et al., 2017). The region experiences a cold, windy tundra climate, with snow cover for most of the year. Ice typically forms in November and persists until June, with mean annual maximum ice thickness of 0.88 m (1960–2023).

Lake Kallavesi is a boreal, oligotrophic, dimictic lake situated in the Finnish lake district at an elevation of 82 m above sea level (Leppäranta & Wen, 2022). It has a surface area of 478 km^2 and has mean and maximum depths of 9.71 and 75 m, respectively (Noori et al., 2022). The region experiences a typical taiga climate, with snow cover persisting for up to 9 months per year. Ice cover generally extends from December through May, with mean annual maximum ice thickness of 0.57 m (1961–2023).

Lake Pyhäjärvi, Eura (also referred to as Pyhäjärvi, Säkylä) is an eutrophic lake in southeastern Finland, situated at 45 m above sea level. It covers 155 km^2 and is relatively shallow, with an average depth of 5.5 m and a maximum depth of 26 m (Ventelä et al., 2016). The region experiences irregular winter snow cover. Ice typically forms from December to March, with mean annual maximum ice thickness of 0.50 m (1992–2023).

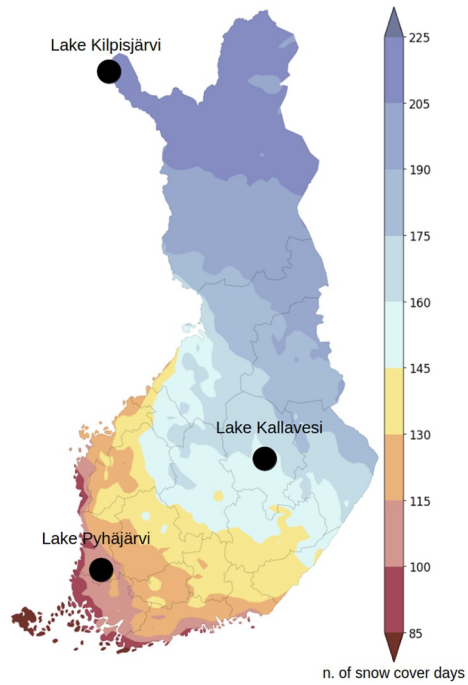

Figure 2. Location of the three lakes used to test the model: Lake Kilpisjärvi, Lake Kallavesi, and Lake Pyhäjärvi. The background map shows the typical number of snow cover days in Finland during the 1991–2020 normal period. Adapted from Finnish Meteorological Institute (2025).

2.5. Available Data

With the integration of the ice module, the *air2water* model requires precipitation in addition to air temperature. The meteorological forcing was obtained from the ERA5 single-level reanalysis provided by the Copernicus Climate Change Service (C3S) at the European Center for Medium-Range Weather Forecasts (ECMF, 2022). We extracted daily 2 m air temperature and accumulated rainfall and snowfall at the 0.25° grid cell nearest to each lake's ice-measurement location, spanning January 1959 to 2023. Snowfall data were also downloaded to enable testing of the model both with and without the internal snowfall estimation algorithm based on parameter a_{12}.

ERA5 reanalysis data offered the continuous forcing required by the model, addressing the spatial and temporal discontinuities often associated with in situ observations. However, reanalysis data must be verified against observations. Where available, we cross-checked the reanalysis against ground station records to assess reliability. In situ air temperature and precipitation were retrieved at a daily frequency from Climate Explorer (www.climexp.knmi.nl), a web-based database maintained by the Royal Netherlands Meteorological Institute (KNMI). For Lake Kilpisjärvi, ERA5 air temperature and precipitation data were compared against measurements from the Enontekiö Kilpisjärvi station (N 69.05, E 20.78; 1959–1979). After 1978, the station was renamed Enontekiö Kilpisjärvi Kyläkeskus, with precipitation records continuing from 1979 through 2024. For Lake Kallavesi, we used combined data from the Kuopio Inkilanmäki (N 62.90, E 27.68; 1959–1998) and Kuopio Savilahti (N 62.89, E 27.64; 2005–2024) stations. No suitable nearby station existed for Lake Pyhäjärvi, so no comparison was performed.

In situ LSWT, ice thickness, and ice timing data used to calibrate the model and assess its performance, were obtained from the Finnish Environmental Institute data set (SYKE, 2025). For Lake Kilpisjärvi, the monitoring stations are named Kilpisjärvi with LSWT data available since 1994 and ice-on/off dates since 1952 (N 69.05, E 20.79), total ice thickness since 1964 and IQ since 2014 (N 69.05, E 20.78). For Lake Kallavesi, the stations are Kallavesi (Kuopio) (N 62.90, E 27.73) with LSWT data since 1960 and ice-on/off dates since 1822, and Kallavesi (Itkonniemi) (N 62.90, E 27.73) with total ice thickness since 1961 and IQ since 2015. For Lake Pyhäjärvi, LSWT is monitored at Säkylän Pyhäjärvi (N 61.11, E 22.17) with data available since 1990; ice thickness is recorded at Pyhäjärvi (Säkylä) (N 61.03, E 22.20) since 1992 with IQ data available from 2015; ice-on/off dates are available from Pyhäjärvi (Kauttua) (N 61.10, E 22.18) with records going back to 1914.

LSWT observations were recorded daily for Kilpisjärvi and Kallavesi, and approximately every 10 days for Pyhäjärvi, all with a reported accuracy of 0.1°C. Ice thickness measurements were taken roughly every 15 days, with a precision of about 1 cm. For this study, observed ice-on and ice-off dates were used to set observed ice thickness to zero at the start and end of each ice season.

The data set was divided into two subsets to support model calibration and validation: the period from 2014 to 2023, during which IQ measurements are available, was used for calibration. The remaining portion of the data set, extending back prior to 2014 depending on data availability for each lake, was reserved for validation.

3. Results

3.1. Validation of Reanalysis Forcing Data

To evaluate the suitability of ERA5 reanalysis data as a substitute for in situ measurements, we compared these data against ground-based observations where available. For Lake Kallavesi (Figure 3), ERA5 air temperature data throughout the annual cycle show excellent agreement with in situ records, with values closely following the 1:1 line, a high coefficient of determination ($R^2 = 0.99$), and minimal scatter (Figure 3a). Comparable results were found for Lake Kilpisjärvi, although with a slight deviation from the 1:1 line and slightly more scatter, likely due to the region's more complex topography, while still maintaining a strong correlation ($R^2 = 0.96$, see Figure S6 in Supporting Information S1). Cold-season (November–May) precipitation comparisons revealed greater variability at the daily scale, yet weekly-averaged ERA5 data showed good agreement with ground-based observations (Figures 3b and 3c and Figures S6b and S6c in Supporting Information S1). Weekly ERA5 precipitation aligned well with the 1:1 line and yielded high R^2 values ranging from 0.79 to 0.83 for Lake Kallavesi, and from 0.49 to 0.57 for Lake Kilpisjärvi, depending on the reference station and time period considered. This level of agreement is satisfactory given the temporal scale of the processes simulated by the model.

3.2. Performance of the Ice Module

The performance of the model in terms of RMSE and ME for all three lakes is presented in Table 1 (see Table S3 in Supporting Information S1 for the performance in terms of NSE), for the six different calibration configurations discussed in Section 2.3. The main results for Lake Kallavesi are presented in Figures 4–6. Corresponding figures for Lake Pyhäjärvi and Lake Kilpisjärvi are available in Supporting Information S1 (see Figures S13–S17 and S22–S26; see also Figures S7 and S8 for the validation period of Lake Kallavesi).

Figure 4 presents heat-map scatter plots comparing observed and simulated data for LSWT during the ice-free season, as well as total, black, and white-ice thickness for Lake Kallavesi. The plots correspond to the six different model configurations analyzed, each displayed in separate rows. Each column corresponds to a different variable: LSWT during the calibration period (LSWT cal.), LSWT during the validation period (LSWT val.), total ice thickness during calibration (h_{tot} cal.), total ice thickness during validation (h_{tot} val.), black-ice thickness during calibration (h_b cal.), and white-ice thickness during calibration (h_w cal.). Results are displayed as heat-map scatter plots, where color intensity reflects the density of data points within each pixel. The black line represents the 1:1 reference line.

Table 1 reports the RMSE values for all six model configurations and for each of the six variables shown in the heat-map scatter plots (Figure 4). Note that validation for black and white-ice thickness is not available, as IQ data were only available after 2014 and were prioritized for model calibration. However, validation was performed for total ice thickness, which provides an integrated measure of ice conditions.

Figure 5 presents time series of observed and simulated variables for Lake Kallavesi, using model calibration based solely on LSWT (i.e., $\beta = 1$). Panel (a) shows the modeled and observed LSWT together with the air temperature used as forcing; panel (b) shows observed and modeled total ice thickness; and panel (c) displays black-ice, white-ice, and snow thickness. The shaded areas represent the range of variation across 10 independent model runs, providing an indication of model stability. The same comparison is provided in Figure 6, but using $\beta = 0.5$ with inclusion of IQ data in the calibration. Below, we discuss in detail these results for LSWT, total ice thickness and timing, and ice-quality thickness.

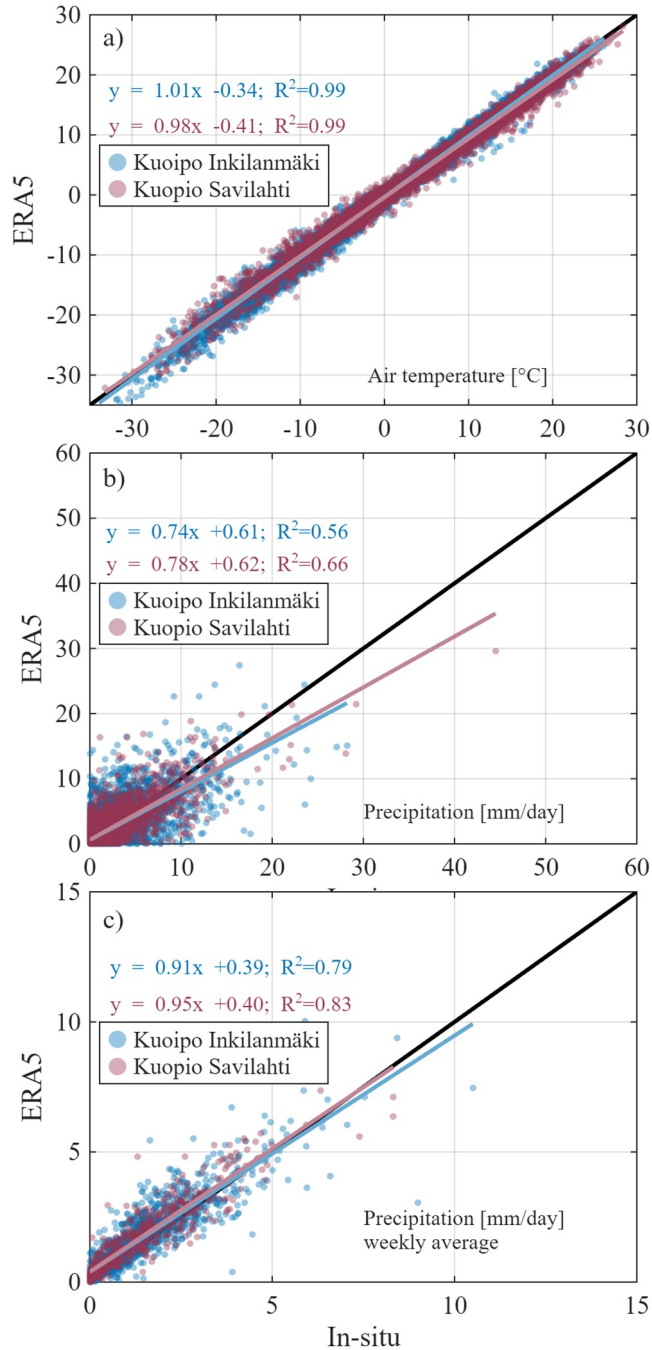

Figure 3. Scatter plots comparing observed (in situ) and modeled (ERA5 reanalysis) meteorological variables for Lake Kallavesi: (a) air temperature, (b) daily precipitation, and (c) weekly precipitation. Different colors represent distinct in situ data sets (see Section 2.5). Colored lines show linear regression fits; the black line indicates the 1:1 reference. Air temperature covers the full annual cycle, while precipitation comparisons are restricted to the cold season (November–May).

Here, we focus on the results obtained using the internal snowfall algorithm based on parameter a_{12} (see Figure S2 in Supporting Information S1). For comparison, the model was also tested without this algorithm, directly using reanalysis-provided snowfall values instead. In the latter case, parameter a_{12} is not used thereby reducing model complexity and epistemic uncertainty. The model's performance remained similar when observed snowfall data were used directly (see Tables S4 and S5 and Figures S10–S12, S18–S20, and S27–S29 in Supporting Information S1).

Table 1
Root Mean Square Error (RMSE) for Lake Surface Water Temperature (LSWT), Total, Black, and White-Ice Thickness, and Mean Error (ME) for Ice-On and Ice-Off Dates

Model configuration	LSWT (°C)	h_{tot} (m)	h_b (m)	h_w (m)	Ice-on (d)	Ice-off (d)
Lake Kallavesi						
air2water 6 par	1.16/1.22	–	–	–	−4/−3	−32/−36
$\beta = 1$	1.16/1.19	0.22/0.23	0.18	0.08	−4/−3	−14/−14
$\beta = 0.5$	1.28/1.23	0.06/0.12	0.09	0.08	−9/−4	0/−4
$\beta = 0.5$ and IQ	1.41/1.38	0.07/0.11	0.08	0.06	−5/−2	+2/−3
$\beta = 0$	8.44/7.12	0.05/0.13	0.10	0.08	−2/+2	+1/−3
$\beta = 0$ and IQ	11.99/10.94	0.07/0.10	0.09	0.06	−17/−9	+4/−1
Lake Pyhäjärvi						
air2water 6 par	0.89/0.90	–	–	–	−18/−15	−31/−33
$\beta = 1$	0.88/0.90	0.17/0.19	0.17	0.07	−18/−15	−17/−20
$\beta = 0.5$	1.12/1.17	0.07/0.11	0.07	0.06	−1/+1	−7/−7
$\beta = 0.5$ and IQ	1.22/1.27	0.08/0.11	0.07	0.04	−2/0	−9/−9
$\beta = 0$	10.25/10.27	0.06/0.11	0.07	0.05	−4/−5	+7/+1
$\beta = 0$ and IQ	9.31/9.30	0.07/0.12	0.07	0.04	+5/+7	+10/+2
Lake Kilpisjärvi						
air2water 6 par	0.90/1.06	–	–	–	+3/0	−41/−46
$\beta = 1$	0.86/1.03	0.17/0.23	0.19	0.17	+3/−1	−16/−17
$\beta = 0.5$	0.96/1.04	0.08/0.15	0.13	0.11	−1/−4	−7/-4
$\beta = 0.5$ and IQ	0.96/1.04	0.12/0.11	0.09	0.10	−1/−4	−7/−3
$\beta = 0$	5.87/5.03	0.07/0.14	0.12	0.11	−4/−6	−3/−1
$\beta = 0$ and IQ	7.93/7.54	0.09/0.11	0.09	0.09	−28/−25	−2/+1

Note. Each column refers to a different variable and each row to a specific calibration configuration, as described in Figure 4. Results are reported as *calibration/validation*, where applicable. If only a single value is shown, it corresponds to the calibration period.

3.2.1. Lake Surface Water Temperature

With the integration of the ice module into the *air2water* model, a primary objectives was to ensure that LSWT predictions remained at least as accurate as those from the original model, with the potential for improvement through better simulation of ice-on and ice-off periods. Therefore, we began by comparing the performance of LSWT simulations from the new model versions against that of the original 6-parameter *air2water* configuration. The original 6-parameter version of *air2water* (*air2water* 6 par.) effectively simulates LSWT, yielding RMSE values of 1.16/0.89/0.90°C for the calibration period and 1.22/0.90/1.06°C for the validation period (mean values for Lake Kallavesi/Pyhäjärvi/Kilpisjärvi respectively; from here on, we present the results for the three lakes in this order). The results exhibit limited scatter in both periods (see Figure 4 for Lake Kallavesi), with minor deviations from the 1:1 line, as indicated by the lighter color density. LSWT prediction improves slightly with the addition of the ice module ($\beta = 1$), obtaining RMSEs equal to 1.16/0.88/0.86 °C and 1.19/0.90/1.03 °C for the calibration and validation periods respectively. Although the overall improvement in RMSE is modest, it is primarily concentrated after the ice-off periods, consistent with the improvement in simulating the ice-off timing (see the next section). Since fewer observations are available for these periods compared to the rest of the year, the effect on overall RMSE remains limited. Nevertheless, improved ice dynamics still yield more accurate LSWT simulations.

When using both LSWT and total ice thickness data for the calibration ($\beta = 0.5$), the performance worsens slightly but the model is still able to accurately predict LSWT: RMSEs are 1.28/1.12/0.96°C and 1.23/1.17/1.04°C for the calibration and validation periods, respectively. In this configuration, the calibration process aims to optimize both LSWT and ice thickness with equal weight, inherently leading to a trade-off between the two

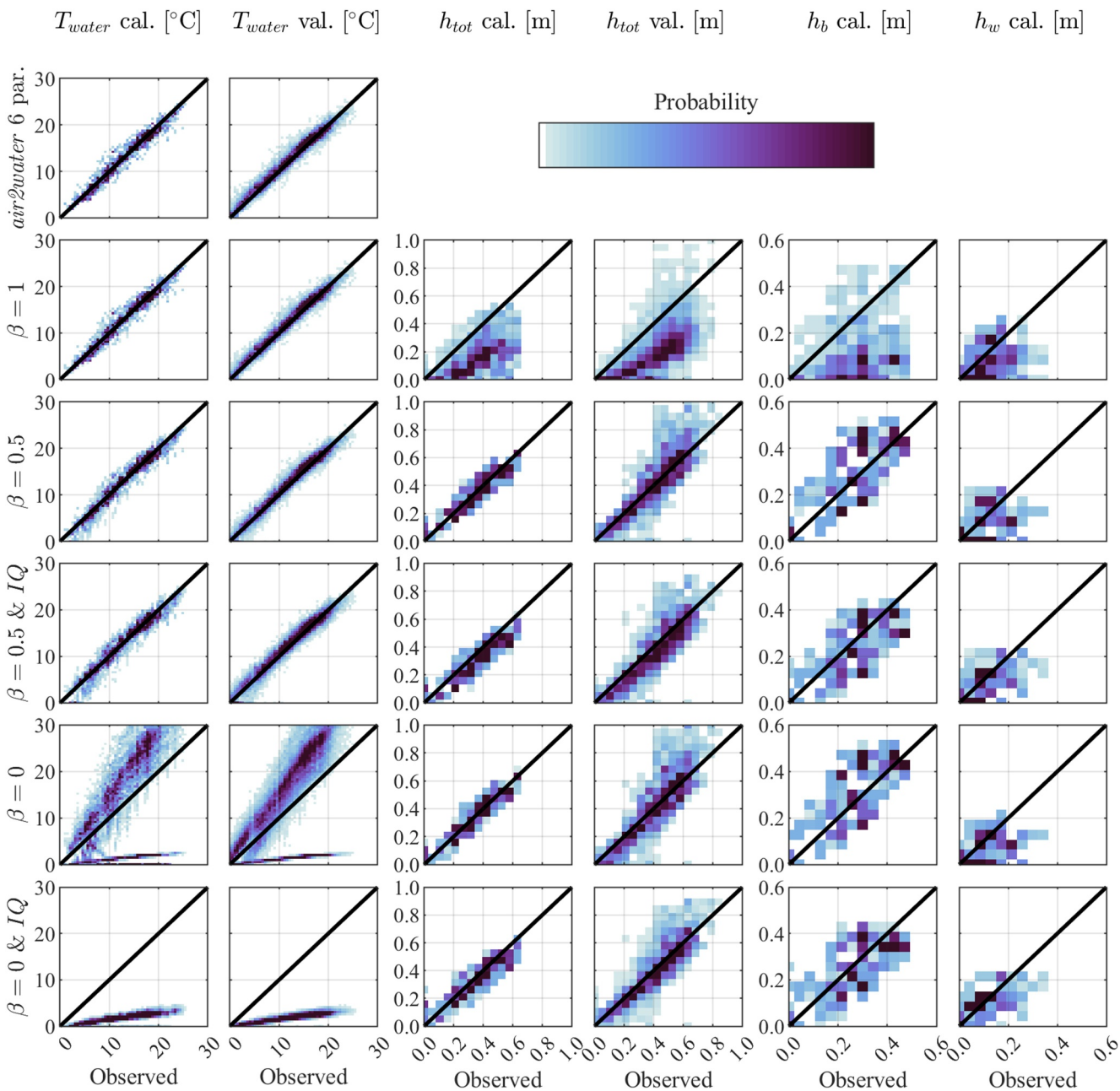

Figure 4. Heat-map scatter plots comparing observed and modeled lake surface water temperature (LSWT) and ice thickness for Lake Kallavesi. Columns show: LSWT (calibration and validation), total ice thickness (calibration and validation), black-ice thickness (calibration), and white-ice thickness (calibration). Rows correspond to six model versions: original six-parameter *air2water*; *air2water* with ice module calibrated using only LSWT ($\beta = 1$); calibrated using LSWT and total ice thickness and using LSWT and black/white-ice thickness ($\beta = 0.5$); calibrated using only total ice thickness and black/white-ice thickness ($\beta = 0$). Colors represent data density; the black line is the 1:1 reference line.

objectives. As a result, a slight reduction in LSWT accuracy is to be expected. When comparing results across the three lakes, the decline in model performance observed for Lake Pyhäjärvi relative to the *air2water* 6 par and $\beta = 1$ configurations is slightly more pronounced than for Kallavesi and Kilpisjärvi. This may be attributed to the lower temporal resolution of the calibration data available for Pyhäjärvi (once every 10 days), which likely provides less constraint for the optimization process compared to the daily measurements available for the other two lakes.

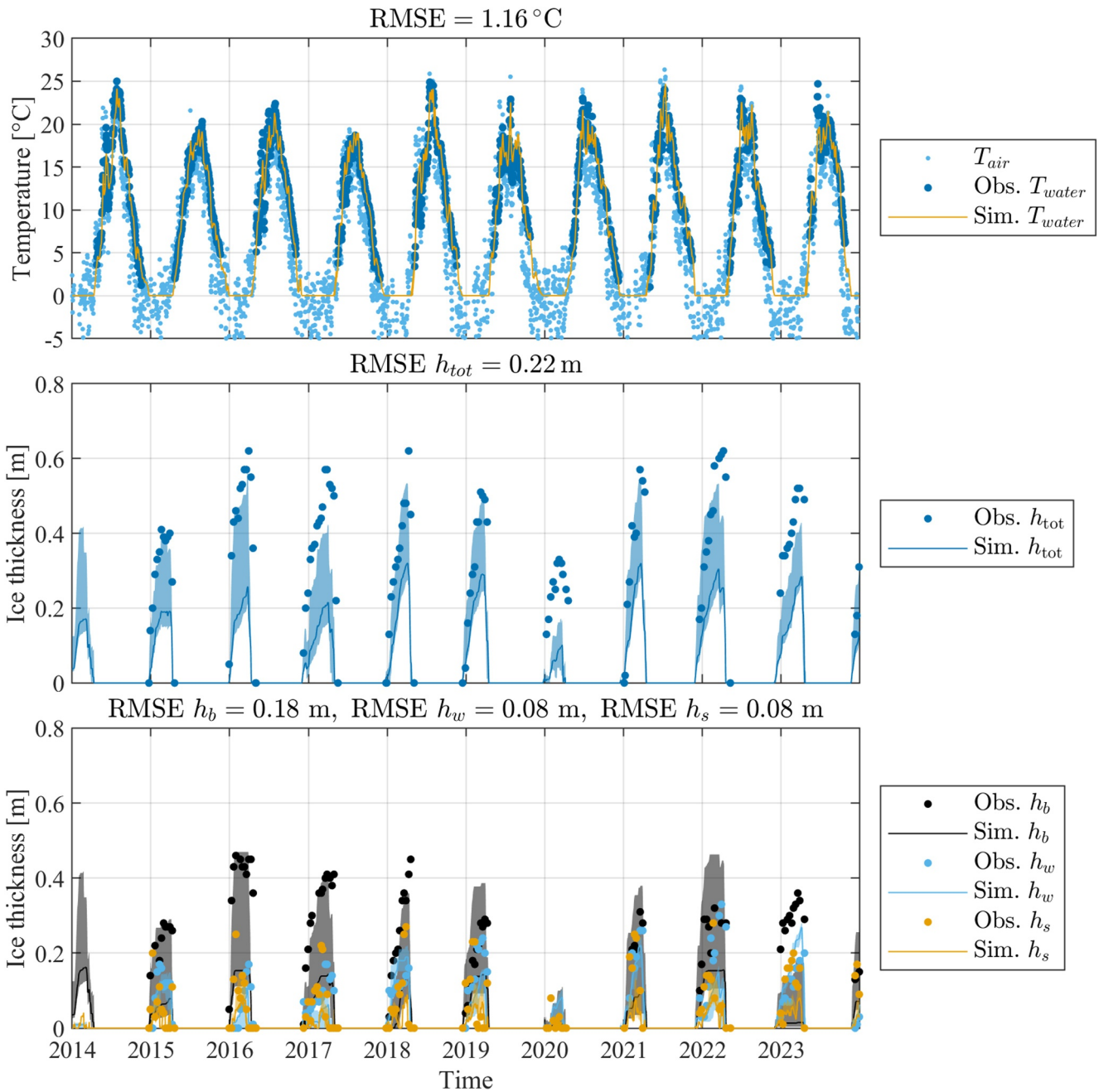

Figure 5. Time series for Lake Kallavesi during the calibration period using lake surface water temperature (LSWT) to calibrate the model ($\beta = 1$): (a) observed and modeled LSWT with air temperature forcing, (b) observed and modeled total ice thickness, and (c) observed and modeled black-ice, white-ice, and snow thickness. The solid lines represent the median values, and the shaded areas denote the range between the 5th and 95th percentiles, illustrating the variability across 10 independent runs.

LSWT dynamics are also accurately simulated when both LSWT and black/white-ice thickness are used for model calibration ($\beta = 0.5$ and IQ; see Figures 4 and 6a). The resulting RMSEs are 1.41/1.22/0.98°C for the calibration period and 1.38/1.27/1.03°C for the validation period.

When using only total ice thickness for calibration ($\beta = 0$ and $\beta = 0$ and IQ), LSWT prediction worsens. LSWT is generally over or underestimated, depending on the lake, and increased scatter is observed around the 1:1 line (Figure 4). The decline in performance is particularly pronounced when only ice-quality data are used for

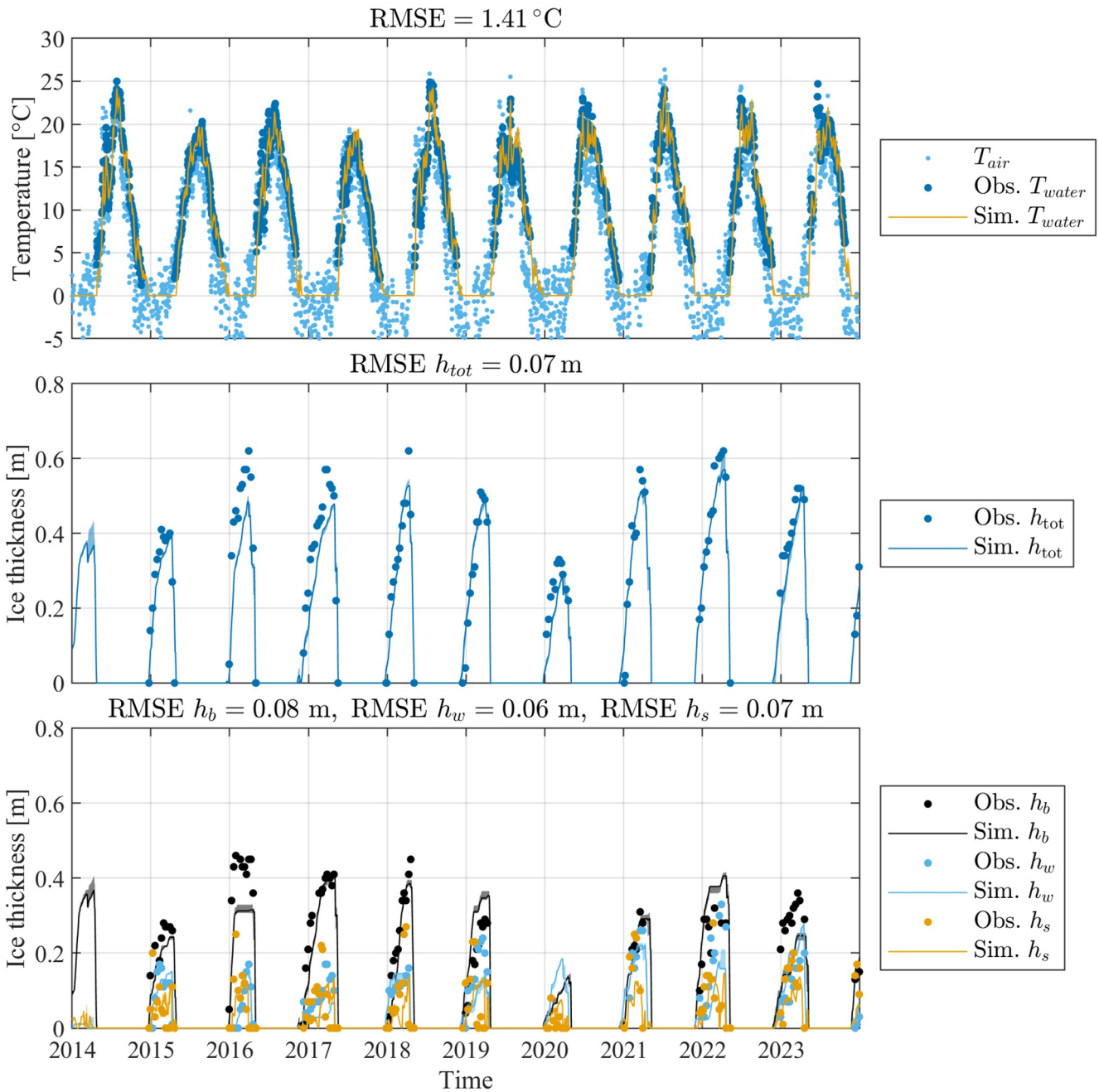

Figure 6. Time series for Lake Kallavesi during the calibration period using lake surface water temperature (LSWT) and black/white ice thickness to calibrate the model ($\beta = 0.5$ and ice quality): (a) observed and modeled LSWT with air temperature forcing, (b) observed and modeled total ice thickness, and (c) observed and modeled black-ice, white-ice, and snow thickness. The solid lines represent the median values, and the shaded areas denote the range between the 5th and 95th percentiles, illustrating the variability across 10 independent runs.

calibration. This low performance is expected, as the model is no longer directly informed by LSWT observations, thus limiting its ability to capture water temperature dynamics.

3.2.2. Total Ice Thickness and Ice Cover Timing

The LSWT-based estimate of ice-on dates produced by the original *air2water* model shows reasonable accuracy: ME of −4/−18/+3 d and −3/−15/0 d (Kallavesi/Pyhäjärvi/Kilpisjärvi) for calibration and validation respectively.

In contrast, ice-off dates tend to be predicted much earlier than observed, reflecting the model's limitations in capturing late-season ice cover without explicit simulation of ice processes. MEs are −32/−31/−40d and −36/−33/−46d for calibration and validation, respectively.

As for *air2water* with the new ice module, when no ice thickness data is used for the calibration ($\beta = 1$), the RMSE values for total ice thickness are moderately high and reach up to 0.22/0.17/0.17 m and 0.23/0.19/0.23 m for calibration and validation respectively. For Lakes Kallavesi and Pyhäjärvi, the width of the range of variation obtained comparing results from the set of 10 simulations is significant (Figure 5b and Figure S14b in Supporting Information S1). Although the magnitude of the error is non-negligible, the model effectively reproduces the ice timing and interannual patterns. The prediction of ice-on dates remains accurate: ME of −4/−18/+3 d and −3/−15/−1 d for calibration and validation respectively; while the prediction of ice-off dates significantly improves: ME of −14/-17/-16 d and −14/-20/-17 d for calibration and validation respectively. In the case of Lake Kallavesi, simulated ice thickness tends to be underestimated, and the heat-map scatter plot shows dispersion around the 1:1 line during both calibration and validation periods (Figure 4). Nonetheless, a simple linear rescaling of model outputs to observations in post-processing brings the model outputs into close agreement with observations (see Figure S9 in Supporting Information S1), suggesting that the model structure reliably simulates ice dynamics. For the other two lakes, the magnitude of simulated ice thickness is already consistent with observations, even without rescaling (Figures S14 and S23 in Supporting Information S1). Overall, this version of the model is particularly interesting, as it captures both the timing and seasonal evolution of ice thickness (at least in relative terms) without relying on ice data for calibration. This is especially relevant given that ice thickness observations are often unavailable, allowing the model to be applied even to lakes lacking such measurements.

When adding total ice thickness measurements to calibrate the model ($\beta = 0.5$), the performance significantly improves. RMSEs for total ice thickness are 0.06/0.07/0.08 m and 0.12/0.11/0.15 m for calibration and validation respectively. Pixels in the heat-map plots are now more tightly distributed around the parity line, with reduced dispersion. A slight deviation from the 1:1 line is observed in the upper-left portion of the scatter plot for Lakes Kallavesi and Kilpisjärvi, suggesting a moderate overestimation of higher ice thickness values (Figure 4 and Figure S22 in Supporting Information S1). The performance in simulating ice-on dates is generally improved, with ME of −9/−1/−1 d and −4/+1/−4 d for calibration and validation respectively. A more substantial and significant improvement is observed for ice-off dates, with ME of 0/−7/−7 d for calibration and −4/−7/−4 d for validation.

Accurate prediction of total ice thickness is achieved also when black and white-ice thickness data are included for model calibration ($\beta = 0.5$ and IQ). The RMSE values are 0.07/0.08/0.12 m and 0.11/0.11/0.11 m for calibration and validation, respectively. Compared to the $\beta = 1$ version, the range of variation obtained across the 10 simulation runs is significantly reduced (Figure 6b and Figure S15b in Supporting Information S1). A similar reduction is observed for $\beta = 0.5$ (Table 1), indicating improved constraint of the ice parameters due to the inclusion of ice observation data. Maximum ice thickness is adequately reproduced, with only slight underestimations in a few years. Accurate simulation of ice cover timing is also retained, consistent with the results obtained for $\beta = 0.5$. For ice-on dates, MEs are −5/–2/–1 d and −2/0/–4 d for calibration and validation, respectively. For ice-off dates, MEs are +2/–9/–7 d and −3/–9/–3 d for calibration and validation, respectively.

Finally, calibrating the model using only ice thickness data (Figure 4) leads to a slight but not significant improvement in performance, with no substantial changes observed compared to the $\beta = 0.5$ and $\beta = 0.5$ and IQ versions. Notably, the $\beta = 0$ and IQ configuration shows a significant deterioration in the prediction of ice-on and ice-off dates (see Table 1).

3.2.3. Ice Quality

Following the good performance in simulating total ice thickness, modeled black and white-ice thicknesses were evaluated against in situ measurements, showing overall good agreement across different *air2water* model versions.

The $\beta = 1$ version simulates black ice with larger errors compared to white ice: RMSEs for black ice are 0.18/0.17/0.19 m and RMSEs for white ice are 0.08/0.07/0.17 m (Kallavesi/Pyhäjärvi/Kilpisjärvi). In line with the total ice thickness results discussed above, both the black-ice and white-ice layers are generally underestimated by the model in Lake Kallavesi. Moreover, in both Lakes Kallavesi and Pyhäjärvi, the variability across the 10

simulation runs is substantial (Figure 5c and Figure S14c in Supporting Information S1). Nonetheless, the overall dynamics are reasonably well captured in all cases, allowing for interannual comparisons in relative terms.

Representation of IQ improves when considering both LSWT and ice thickness data to calibrate the model ($\beta = 0.5$ and $\beta = 0.5$ and IQ). RMSEs obtained with $\beta = 0.5$ are 0.09/0.07/0.13 m and 0.08/0.06/0.11 m for black and white ice, respectively. For the $\beta = 0.5$ and IQ configuration, RMSEs are 0.08/0.07/0.09 m for black ice and 0.06/0.04/0.10 m for white ice. In both cases, heat map plots show values closely aligning along the parity line, with low scatter (Figure 4). As observed for total ice thickness, for Lakes Kallavesi and Pyhäjärvi the range of variation across the set of 10 simulation runs is significantly reduced (Figure 6c and Figure S15c in Supporting Information S1), with the model capturing both seasonal evolution and interannual variability. Snow depth dynamics are also reasonably well represented, although accumulation and melt events are not always captured in full detail.

When calibrating the model using only ice thickness data (versions $\beta = 0$ and $\beta = 0$ and IQ), the simulation of black and white-ice thickness shows only minor changes compared to the previous configurations, as also observed for total ice thickness (Table 1, Figure 4).

The model's performance in simulating IQ improves with decreasing latitude across the three lakes. The (slightly) lower performance observed for the northernmost Lake Kilpisjärvi is expected, as higher snowfall increases the influence of snow cover on both white-ice formation and black-ice growth. While the model includes white-ice formation and snow insulation, it simplifies snow properties by assuming constant thermal conductivity and density, even though these characteristics vary with snow accumulation as a result of compaction processes. Furthermore, in regions with heavy snowfall, accurately simulating real conditions remains particularly challenging, as precipitation data alone cannot adequately capture local snow accumulation and wind-driven redistribution. Using snowfall estimates directly from reanalysis data sets, rather than relying on the internal temperature-based classification algorithm governed by parameter a_{12}, does not substantially improve ice simulation performance. This suggests that epistemic uncertainty arising from model structure along with unresolved spatial variability of snow due to local effects, remains the limiting factors (see Figures S10–S12, S18–S20, and S27–S29 in Supporting Information S1). Additional uncertainties may also arise from measurement limitations, as the observation of ice layers is affected by intrinsic ambiguities in separating and quantifying black ice, white ice, and snow layers.

3.3. Model's Parameters Across Calibration Configurations

Figure 7 presents box plots of model parameters (standard *air2water* parameters a_1 to a_6 and newly included ice module parameters a_9 to a_{12}) for Lake Kallavesi across the different model configurations examined above. The box plots summarize the distribution of parameter values obtained from the 10 independent runs per configuration.

The results indicate that the standard *air2water* parameters a_1 to a_6 remain relatively stable across configurations, although some shifts and increased variability are observed, particularly when ice data are included in the calibration. Notably, for $\beta = 0.5$ the parameters' deviations from the *air2water* 6 par. configuration are small, suggesting that these parameter values (describing the heat exchange between the atmosphere and the lake surface, whether water or ice) remain consistent even when the ice module and total ice data are included. In contrast, for $\beta = 0$ the deviations and the variability are significantly larger, which is expected due to the sensitivity arising from the trade-off between fitting water and ice data. Parameters associated to the ice module a_9 to a_{12} also demonstrate reasonable stability across configurations, with higher variability across runs particularly when ice data are excluded from calibration ($\beta = 1$). This is expected due to the reduced constraints on these parameters under this calibration configuration. Additionally, substantial variability is observed in the case $\beta = 0$ and IQ. In general, the inclusion of IQ data tends to increase variability in all model's parameters, reflecting uncertainties introduced by limited data availability and observational challenges related to ambiguities or measurement errors in identifying and quantifying the different ice layers. Interestingly, parameter a_{11} is typically lower than unity, consistent with the higher albedo of ice and the reduced turbulent transfer coefficients, both of which decrease heat exchange relative to open-water conditions. Overall, similar considerations can be drawn from the boxplots relative to Lake Pyhäjärvi and Lake Kilpisjärvi (see Figures S21 and S30 in Supporting Information S1). Finally, in some cases parameter estimates approach their a priori bounds, as obtained by

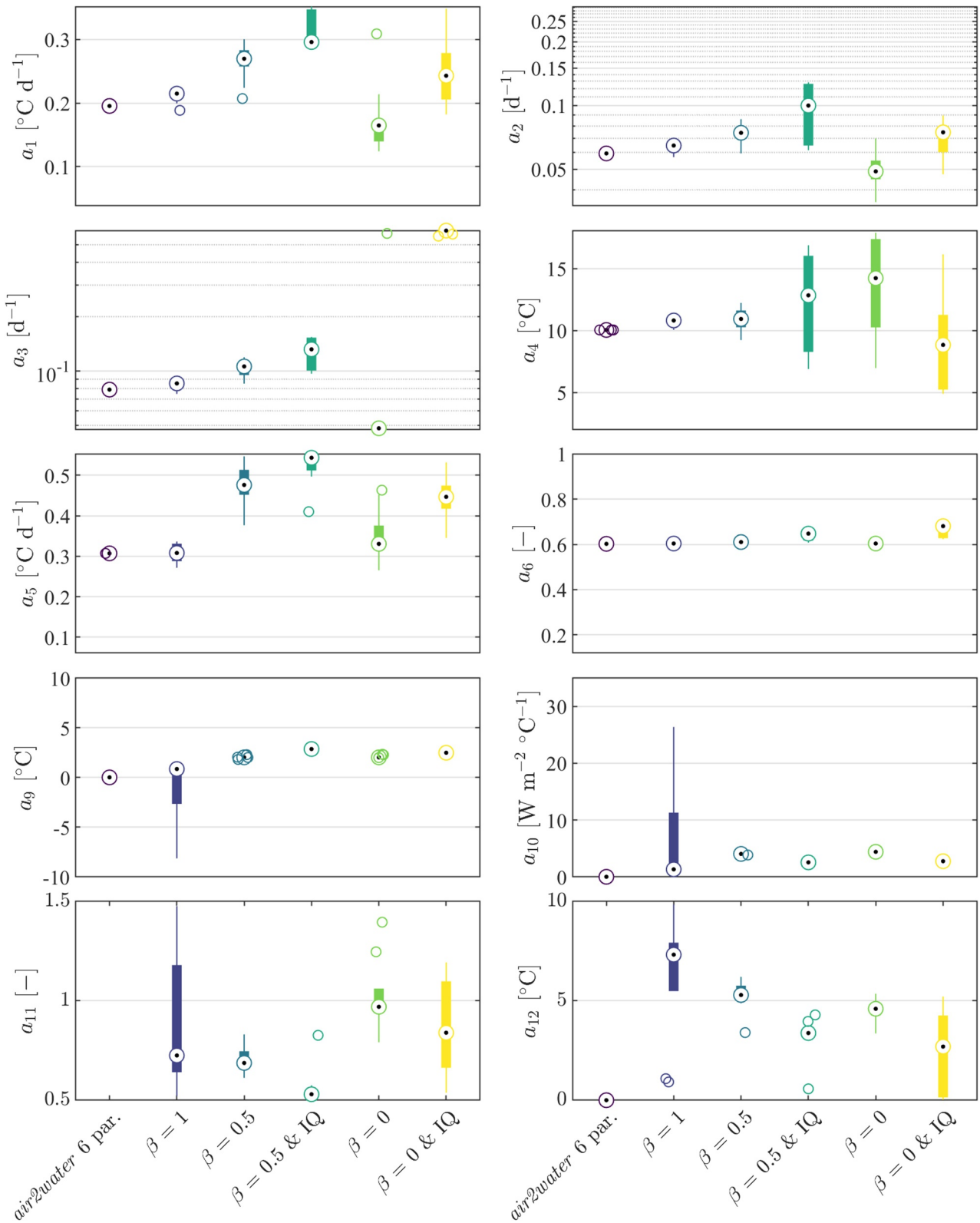

Figure 7. Box plots of parameter values (standard *air2water* parameters a_1 to a_6 and newly included ice module parameters a_9 to a_{12}) for Lake Kallavesi, based on 10 independent runs and for each calibration configuration as indicated on the *x*-axis.

narrowing after the first calibration run (see Section 2.3). This is considered an acceptable compromise between allowing sufficient flexibility for the parameters to be informed by the available data and maintaining physical interpretability.

4. Discussion

The *air2water* model has been widely recognized as a simple yet effective tool for predicting LSWT using only air temperature data, and has shown better performance than various alternative approaches, including machine learning, statistical, and one-dimensional models (see e.g., Heddam et al., 2020; Piccolroaz et al., 2018; Zhu et al., 2020). The integration of the ice module introduced in this study enables the model to reliably simulate ice timing, thickness, and quality, using only minimal input data: air temperature, precipitation, and an approximate value for the lake's mean depth.

The performance achieved by the *air2water* model combined with the new ice module is consistent with values reported in the literature for more complex models. For example, applications of the FLake model (Mironov, 2008) have reported RMSE values below 2°C for LSWT across temperate, boreal, and arctic lakes of varying depth and ice cover (Golub et al., 2022), and errors around 10 cm for total ice thickness in shallow temperate lakes (de Bruijn et al., 2014). Similarly, applications of the model Simstrat (Goudsmit et al., 2002) have reported RMSE values under 1.5°C for LSWT (Golub et al., 2022), and errors of approximately 10 cm for ice thickness in temperate reservoirs and lakes (Kobler & Schmid, 2019). The performance is thus comparable, which is especially notable considering that these other models generally rely on a wider range of meteorological inputs, while the approach presented here maintains a low-complexity structure without a loss in accuracy.

A key finding is that LSWT prediction improves consistently across all three lakes when comparing the original six-parameter version of the model (*air2water* 6-par) to the updated version incorporating the ice module, calibrated using LSWT data only ($\beta = 1$). This improvement demonstrates that the added module enhances model performance for LSWT simulations, providing evidence of the robustness and sound structure of the ice module.

The ability to obtain reliable predictions of water temperature, ice thickness, and ice phenology using only two meteorological input variables represents a particularly advantageous feature of the model. This is especially relevant given that the required inputs, air temperature and precipitation, are among the most commonly measured parameters by ground-based weather stations and are therefore widely available. Moreover, these variables are included in most climate model outputs, making the model a valuable tool for estimating LSWT and ice cover dynamics in ensemble projections under future climate scenarios. One potential limitation of this limited-input approach is the absence of explicit solar forcing, which may play a key role in lake ice dynamics, particularly during the melting season. In the model, solar radiation is implicitly represented through air temperature and through the calibration of parameters a_5 and a_6, which define the amplitude and phase of a sinusoidal component of the heat budget that encompasses solar radiation, among other annually varying drivers. While this indirect representation may limit the model's ability to simulate short-term variations in melting driven by rapid changes in solar radiation, it generally reproduces seasonal ice dynamics well.

A more comprehensive assessment of the model's potential could be achieved through applications beyond Finland, including lakes from diverse climatic regions and with varying ice column composition. Such applications would offer the opportunity to further explore the model's ability to represent differences in white-ice formation and black-ice growth under contrasting environmental conditions. In particular, testing the model on lakes at latitudes where ice cover forms only intermittently, or in regions with limited or absent snowfall (e.g., Central Asia), could provide useful insights into its capacity to simulate interannual variability in ice formation and IQ. In this context, a systematic large-scale application, similar to previous efforts with the original *air2water* model (Piccolroaz, 2020), may help identify general performance-related patterns and explore the potential for regionalizing model parameters based on morphological or climatic lake attributes. Such an approach could enhance the model's usability in data-scarce regions by reducing the need for extensive site-specific calibration. A regionalization framework, such as that proposed by Toffolon et al. (2014) for the original *air2water* model, could be used to establish empirical relationships between model parameters and key lake characteristics. Future research should therefore explore how these parameters vary with factors such as lake surface area, mean depth, altitude, latitude, climatic zone etc. Finally, future investigations could assess the extent to which calibration data availability, in terms of time series length and temporal resolution, influences the accuracy of model predictions.

Beyond assessing model performance, future improvements could be considered to further enhance its predictive capabilities. One current simplification lies in the treatment of some physical properties of ice and snow, such as thermal conductivities and snow density, which are assumed to be constant. For example, the model uses a fixed thermal conductivity value for ice, corresponding to pure ice. In reality, this property can vary with temperature, air bubble content, and, in saline lakes, also with salinity (Leppäranta, 1983). Similarly, snow thermal conductivity is held constant in the model, even though it depends on snow density, another property currently assumed constant. However, snow density can vary considerably over time due to processes such as metamorphism and compaction, typically ranging from 0.1 to 0.4 g cm^{-3}. This leads to variations in thermal conductivity of up to an order of magnitude (Leppäranta, 1993), affecting heat exchange between the atmosphere and the ice and influencing black-ice growth. Previous studies have shown that accounting for the temporal evolution of snow density can improve the accuracy of simulated ice formation and growth (Leppäranta, 1983). While including such variability would likely enhance the representation of heat transfer processes within the ice layer, it would also increase model complexity. In line with the model's low-complexity philosophy, we opted for a compromise: keeping the number of parameters limited and using representative constant values for the above-mentioned physical properties, while retaining the flexibility to incorporate more detailed or lake-specific formulations in customized versions of the model, if needed.

Another simplification in the model concerns the representation of white ice and slush as single, uniform layers. In reality, multiple layers can form when new snow accumulates on top of an existing white-ice layer before the underlying slush has completely frozen (Saloranta, 2000). While this approach may not capture the full vertical complexity of these layers, it offers a practical balance between realism and model simplicity, and still allows for a reasonable approximation of their thermal and mechanical behavior in most cases. Along the same pragmatic lines, the model addresses occasional inconsistencies during melting conditions by maintaining ice thickness values at their previous time step whenever negative heat fluxes are calculated during a melting phase situations which, although rare, could otherwise lead to conflicting simulations of ice growth and melt. This straightforward solution fits within the overall low-complexity framework of the model.

Overall, in its current configuration, the *air2water* model with the integrated ice module proves to be a reliable tool for predicting ice timing, thickness, and quality in lakes. Future research could leverage the model to explore ice cover-related processes across various disciplines. In fact, as noted earlier in this manuscript, lake ice dynamics affect not only thermodynamic processes but also physical, ecological, biological, and biogeochemical systems. Applying the model in these diverse fields may offer valuable insights into the broader impacts of ice cover and its variability on lake environments.

5. Conclusions

This work focused on the simulation of lake ice timing and thickness by developing and applying an ice module integrated into the existing *air2water* model (Piccolroaz et al., 2013). Originally designed to simulate LSWT using only air temperature as input, *air2water* combines physically based and statistical components in a parsimonious framework. In designing the ice module, the goal was to preserve the core strengths of the original model, namely simplicity, low data requirements, and physical consistency, while extending its capabilities to include ice processes. The resulting module retains these features: it requires only air temperature, precipitation, and a rough estimate of lake mean depth as input, relies on just two equations and four additional parameters to simulate ice growth and melt, and maintains a performance level comparable to that reported in the literature for more complex deterministic models.

After presenting the derivation of the ice module, the model was applied to simulate LSWT and ice cover dynamics in three Finnish lakes: Lake Kallavesi, Lake Kilpisjärvi, and Lake Pyhäjärvi. These lakes were chosen for their contrasting climatic conditions, particularly in terms of snow cover duration, providing an opportunity to assess model performance under different snow regimes. The analysis was carried out using six model configurations, each reflecting a different combination of available calibration data and user priorities, including LSWT, total ice thickness, and IQ.

Results show that the integration of the ice module into the *air2water* model significantly enhances its predictive capabilities. With the exception of configurations calibrated exclusively on ice thickness data, high accuracy in LSWT simulation is maintained or even improved throughout the year. The key added value of the ice module,

however, lies in its ability to simulate ice cover dynamics. All model configurations provide adequate to accurate estimates of ice thickness, timing, and quality with RMSE typically on the order of 10 cm or less. Notably, the model delivers reasonable performance even when no ice data are used for calibration. This is particularly important given the limited availability of ice thickness observations, and it supports the applicability of the model in data-scarce lakes. The accurate estimation of IQ is also especially promising, as it opens the possibility to investigate ice safety and enables the model's use in a broad range of applications involving physical, biological, ecological, and biogeochemical processes under ice cover.

A major strength of the model lies in its reliance on only air temperature and precipitation, two variables that are widely measured by ground stations and included in most climate model outputs. This makes *air2water* a practical and well-suited tool for estimating LSWT and ice cover dynamics, including under future climate change scenarios. Despite its simplicity, the model performs comparably to more complex lake ice models that require a broader set of meteorological inputs, highlighting its competitiveness and versatility.

Overall, the extended *air2water* model offers a robust, parsimonious, and versatile tool for simulating lake thermal and ice dynamics. Its simplicity, combined with competitive performance and minimal input requirements, makes it well suited for large-scale applications, long-term studies, and interdisciplinary research on lake responses to climate variability and change.

Conflict of Interest

The authors declare no conflicts of interest relevant to this study.

Data Availability Statement

The script of the extended *air2water* model, including the ice module, is made available by Piccolroaz et al. (2025) at https://doi.org/10.5281/zenodo.16898866. The repository also contains the input data used to run the model for Lakes Kallavesi, Pyhäjärvi, and Kilpisjärvi.

Acknowledgments
SP acknowledges the Italian Ministry of Universities and Research (MUR), in the framework of the project DICAM-EXC (Departments of Excellence 2023–2027, Grant L232/2016). MF is grateful to the Vilho Yrjö, and Kalle Väisälä Foundation for their kind support for funding. The work was also supported by the EU Horizon Europe–Framework Programme for Research and Innovation (no. 101056921 (GreenFeedBack)) and ICOS-Finland funded by University of Helsinki. Open access publishing facilitated by Università degli Studi di Trento, as part of the Wiley - CRUI-CARE agreement.

References

Ashton, G. D. (1980). Theory of thermal control and prevention of ice in rivers and lakes. *Advances in Hydroscience*, *13*, 131–185. https://doi.org/10.1016/B978-0-12-021813-4.50008-1

Ashton, G. D. (1989). Thin ice growth. *Water Resources Research*, *25*(3), 564–566. https://doi.org/10.1029/WR025i003p00564

Barnes, H. T. (1928). *Ice engineering*. Renouf.

Beyene, M. T., & Jain, S. (2020). Climate-related thresholds in lake ice and the associated environmental and social systems. *Water Security*, *10*, 100065. https://doi.org/10.1016/j.wasec.2020.100065

Cheng, B. (2017). On the numerical resolution in a thermodynamic sea-ice model. *Journal of Glaciology*, *48*(161), 301–311. https://doi.org/10.3189/172756502781831449

Cheng, B., Launianen, J., & Vihma, T. (2003). Modelling of superimposed ice formation and sub-surface melting in the Baltic sea. *Geophysica*, *39*(1–2), 31–50.

Culpepper, J., Jakobsson, E., Weyhenmeyer, G. A., Hampton, S. E., Obertegger, U., Shchapov, K., et al. (2024). Lake ice quality in a warming world. *Nature Reviews Earth & Environment*, *5*(10), 671–685. https://doi.org/10.1038/s43017-024-00590-6

Culpepper, J., Sharma, S., Gunn, G., Magee, M. R., Meyer, M. F., Anderson, E. J., et al. (2025). One-hundred fundamental, open questions to integrate methodological approaches in lake ice research. *Water Resources Research*, *61*(5), e2024WR039042. https://doi.org/10.1029/2024WR039042

de Bruijn, E. I. F., Bosveld, F. C., & van der Plas, E. V. (2014). An intercomparison study of ice thickness models in the Netherlands. *Tellus A: Dynamic Meteorology and Oceanography*, *66*(1), 21244. https://doi.org/10.3402/tellusa.v66.21244

Duguay, C. R., Flato, G. M., Jeffries, M. O., Ménard, P., Morris, K., & Rouse, W. R. (2003). Ice-cover variability on shallow lakes at high latitudes: Model simulations and observations. *Hydrological Processes*, *17*, 3465–3483. https://doi.org/10.1002/hyp.1394

ECMF. (2022). European Centre for medium-range weather forecasts. Retrieved from https://www.ecmwf.int/

Finnish Meteorological Institute. (2025). Snow statistics. Retrieved from https://en.ilmatieteenlaitos.fi/snow-statistics

Flaim, G., Andreis, D., Piccolroaz, S., & Obertegger, U. (2020). Ice cover and extreme events determine dissolved oxygen in a placid mountain lake. *Water Resources Research*, *56*(9), e2020WR027321. https://doi.org/10.1029/2020WR027321

Gaudard, A., man Vinnå, L. R., Bärenbold, F., Schmid, M., & Bouffard, D. (2019). Toward an open access to high-frequency lake modeling and statistics data for scientists and practitioners—The case of swiss lakes using simstrat v2.1. *Geoscientific Model Development*, *12*(9), 3955–3974. https://doi.org/10.5194/gmd-12-3955-2019

Golub, M., Thiery, W., Marcé, R., Pierson, D., Vanderkelen, I., Mercado-Bettin, D., et al. (2022). A framework for ensemble modelling of climate change impacts on lakes worldwide: The ISIMIP lake sector. *Geoscientific Model Development*, *15*(11), 4597–4623. https://doi.org/10.5194/gmd-15-4597-2022

Goudsmit, G.-H., Burchard, H., Peeters, F., & Wüest, A. (2002). Application of k-ε turbulence models to enclosed basins: The role of internal seiches. *Journal of Geophysical Research*, *107*(C12), 23-1–13. https://doi.org/10.1029/2001JC000954

Hampton, S. E., Powers, S. M., Dugan, H. A., Knoll, L. B., McMeans, B. C., Meyer, M. F., et al. (2024). Environmental and societal consequences of winter ice loss from lakes. *Science*, *386*(6718), eadl3211. https://doi.org/10.1126/science.adl3211

Hazem, U. A., & Cary, D. T. (2025). A deep learning approach for modeling and hindcasting lake Michigan ice cover. *Journal of Hydrology*, *649*, 132445. https://doi.org/10.1016/j.jhydrol.2024.132445

He, X., Andreadis, K. M., Roy, A. H., Langhorst, T., Kumar, A., & Butler, C. S. (2025). Modeling daily ice cover in northern hemisphere lakes with a long short-term memory neural network. *Geophysical Research Letters*, *52*(12), e2024GL113544. https://doi.org/10.1029/2024GL113544

Heddam, S., Ptak, M., & Zhu, S. (2020). Modelling of daily lake surface water temperature from air temperature: Extremely randomized trees (ERT) versus Air2Water, Mars, M5Tree, RF and MLPNN. *Journal of Hydrology*, *588*, 125130. https://doi.org/10.1016/j.jhydrol.2020.125130

Heinilä, K., Mattila, O.-P., Metsämäki, S., Väkevä, S., Luojus, K., Schwaizer, G., & Koponen, S. (2021). A novel method for detecting lake ice cover using optical satellite data. *International Journal of Applied Earth Observation and Geoinformation*, *104*, 102566. https://doi.org/10.1016/j.jag.2021.102566

Huang, L., Timmermann, A., Lee, S.-S., Rodgers, K. B., Yamaguchi, R., & Chung, E.-S. (2022). Emerging unprecedented lake ice loss in climate change projections. *Nature Communications*, *13*(1), 5798. https://doi.org/10.1038/s41467-022-33495-3

Huang, W., Zhang, Z., Li, Z., Leppäranta, M., Arvola, L., Song, S., et al. (2021). Under-ice dissolved oxygen and metabolism dynamics in a shallow lake: The critical role of ice and snow. *Water Resources Research*, *57*(5), e2020WR027990. https://doi.org/10.1029/2020WR027990

Imrit, M. A., & Sharma, S. (2021). Climate change is contributing to faster rates of lake ice loss in lakes around the northern hemisphere. *Journal of Geophysical Research: Biogeosciences*, *126*(7), e2020JG006134. https://doi.org/10.1029/2020JG006134

Jankowski, T., Livingstone, D. M., Bührer, H., Forster, R., & Niederhauser, P. (2006). Consequences of the 2003 European heat wave for lake temperature profiles, thermal stability, and hypolimnetic oxygen depletion: Implications for a warmer world. *Limnology & Oceanography*, *51*(2), 815–819. https://doi.org/10.4319/lo.2006.51.2.0815

Jansen, J., Macintyre, S., Barret, D., Chin, Y.-P., Cortés, A., Forrest, A. L., & Schwefel, R. (2021). Winter limnology: How do hydrodynamics and biogeochemistry shape ecosystems under ice? *Biogeosciences*, *126*(6). https://doi.org/10.1029/2020JG006237

Jordan, R. E. (1991). *A one-dimensional temperature model for a snow cover: Technical documentation for SNTHERM (Technical Report)* (Vol. 89). Cold Regions Research and Engineering Laboratory (U.S.), Engineer Research and Development Center (U.S.).

Kelley, D. E. (1997). Convection in ice-covered lakes: Effects on algal suspension. *Journal of Plankton Research*, *19*(12), 1859–1880. https://doi.org/10.1093/plankt/19.12.1859

Kennedy, J., & Eberhart, R. (1995). Particle swarm optimization. *Proceedings of ICNN'95 - International Conference on Neural Networks*, *4*, 1942–1948. https://doi.org/10.1109/ICNN.1995.488968

Kirillin, G., Leppäranta, M., Terzhevik, A., Granin, N., Bernhardt, J., Engelhardt, C., et al. (2012). Physics of sea-sonally ice-covered lakes: A review. *Aquatic Sciences*, *74*(4), 659–682. https://doi.org/10.1007/s00027-012-0279-y

Knoll, L. B., Sharma, S., Denfeld, B. A., Flaim, G., Hori, Y., Magnuson, J. J., et al. (2019). Consequences of lake and river ice loss on cultural ecosystem services. *Limnology and Oceanorgaphy*, *4*(5), 119–131. https://doi.org/10.1002/lol2.10116

Kobler, U. G., & Schmid, M. (2019). Ensemble modelling of ice cover for a reservoir affected by pumped-storage operation and climate change. *Hydrological Processes*, *33*(20), 2676–2690. https://doi.org/10.1002/hyp.13519

Launiainen, J., & Cheng, B. (1998). Modelling of ice thermodynamics in natural water bodies. *Cold Regions Science and Technology*, *27*(3), 153–178. https://doi.org/10.1016/S0165-232X(98)00009-3

Leppäranta, M. (1983). A growth model for black ice, snow ice and snow thickness in subarctic basins. *Nordic Hydrology*, *14*(2), 59–70. https://doi.org/10.2166/nh.1983.0006

Leppäranta, M. (1993). A review of analytical models of sea-ice growth. *Atmosphere-Ocean*, *31*(1), 123–138. https://doi.org/10.1080/07055900.1993.9649465

Leppäranta, M. (2015). *Freezing of Lakes and the evolution of their ice cover*. Springer.

Leppäranta, M., & Kosloff, P. (2000). The thickness and structure of lake pääjärvi ice. *Geophysica*, *36*(1–2), 233–248.

Leppäranta, M., Lindgren, E., & Shirasawa, K. (2017). The heat budget of Lake Kilpisjärvi in the Arctic tundra. *Hydrology Research*, *48*(4), 969–980. https://doi.org/10.2166/nh.2016.171

Leppäranta, M., & Wen, L. (2022). Ice phenology in eurasian lakes over spatial location and altitude. *Water*, *14*(7), 1037. https://doi.org/10.3390/w14071037

Livingstone, D., & Lotter, A. (1998). The relationship between air and water temperatures in lakes of the Swiss Plateau: A case study with palæolimnological implications. *Journal of Paleolimnology*, *19*(2), 181–198. https://doi.org/10.1023/a:1007904817619

Martynov, A., Sushama, L., & Laprise, R. (2010). Simulation of temperate freezing lakes by one-dimensional lake models: Performance assessment for interactive coupling with regional climate models. *Boreal Environment Research*, *15*, 143–164.

McCombie, A. (1959). Some relations between air temperatures and the surface water temperatures of lakes. *Limnology & Oceanography*, *4*(3), 252–258. https://doi.org/10.4319/lo.1959.4.3.0252

Mironov, D. (2008). Parameterization of lakes in numerical weather prediction. Description of a lake model no 11. In *COSMO Technical Report (47)*.

Nash, J. E., & Sutcliffe, J. V. (1970). River flow forecasting through conceptual models. Part i-a discussion of principles. *Journal of Hydrology*, *27*(3), 282–290. https://doi.org/10.1016/0022-1694(70)90255-6

Noori, R., Bateni, S. M., Saari, M., Almazroui, M., & Haghighi, A. T. (2022). Strong warming rates in the surface and bottom layers of a boreal lake: Results from approximately six decades of measurements (1964-2020). *Earth and Space Science*, *9*(2), e2021EA001973. https://doi.org/10.1029/2021EA001973

Perroud, M., Goyette, S., Martynov, A., Beniston, M., & Anneville, O. (2009). Simulation of multiannual thermal profiles in deep Lake Geneva: A comparison of one-dimensional lake models. *Limnology & Oceanography*, *54*(5), 1574–1594. https://doi.org/10.4319/lo.2009.54.5.1574

Piccolroaz, S. (2016). Prediction of lake surface temperature using the air2water model: Guidelines, challenges, and future perspectives. *Advances in Oceanography and Limnology*, *7*(1), 36–50. https://doi.org/10.4081/aiol.2016.5791

Piccolroaz, S. (2020). Global reconstruction of twentieth century lake surface water temperature reveals different warming trends depending on the climatic zone. *Climate Change*, *160*(3), 1–16. https://doi.org/10.4081/aiol.2016.5791

Piccolroaz, S., Fregona, M., Leppäranta, M., Jansen, J., Ala-Könni, J., & Mammarella, I. (2025). Spiccolroaz/Air2Water-Ice: Air2Water+Ice v1.0.0. *Zenodo*. https://doi.org/10.5281/zenodo.16898866

Piccolroaz, S., Healey, N. C., Lenters, J. D., Schladow, S. G., Hook, S. J., Sahoo, G. B., & Toffolon, M. (2018). On the predictability of lake surface temperature using air temperature in a changing climate: A case study for lake Tahoe (U.S.A.). *Limnology & Oceanography*, *63*(1), 243–261. https://doi.org/10.1002/lno.10626

Piccolroaz, S., & Toffolon, M. (2018). The fate of lake Baikal: How climate change may alter deep ventilation in the largest lake on earth. *Climate Change*, *150*(3), 181–194. https://doi.org/10.1007/s10584-018-2275-2

Piccolroaz, S., Toffolon, M., & Majone, B. (2013). A simple lumped model to convert air temperature into surface water temperature in lakes. *Hydrology and Earth System Sciences*, *17*(8), 3323–3338. https://doi.org/10.5194/hess-17-3323-2013

Piccolroaz, S., Zhu, S., Ladwig, R., Carrea, L., Oliver, S., Piotrowski, A. P., et al. (2024). Lake water temperature modeling in an era of climate change: Data sources, models, and future prospects. *Reviews of Geophysics*, *62*(1), e2023RG000816. https://doi.org/10.1029/2023RG000816

Pringle, D. J., Trodahl, H. J., & Haskell, T. G. (2006). Direct measurement of sea ice thermal conductivity: No surface reduction. *Journal of Geophysical Research*, *111*(C5), 16. https://doi.org/10.1029/2005JC002990

Saloranta, T. M. (2000). Modeling the evolution of snow, snow ice and ice in the Baltic sea. *Tellus, Series A: Dynamic Meteorology and Oceanography*, *52*(1), 93–108. https://doi.org/10.3402/tellusa.v52i1.12255

Sharma, S., Blagrave, K., Magnuson, J. J., O'Reilly, C. M., Oliver, S., Batt, R. D., et al. (2019). Widespread loss of lake ice around the northern hemisphere in a warming world. *Nature Climate Change*, *9*(3), 227–231. https://doi.org/10.1038/s41558-018-0393-5

Sharma, S., Blagrave, K., Watson, S. R., O'Reilly, C. M., Batt, R., Magnuson, J. J., et al. (2020). Increased winter drownings in ice-covered regions with warmer winters. *PLoS One*, *15*(11), e0241222. https://doi.org/10.1371/journal.pone.0241222

Sharma, S., En, S., Walker, C., & Ackson, D. O. A. J. (2008). Empirical modelling of lake water-temperature relationships: A comparison of approaches. *Freshwater Biology*, *53*, 897–911. https://doi.org/10.1111/j.1365-2427.2008.01943.x

Sharma, S., Shchapov, K., Culpepper, J., & Magnsuon, J. J. (2024). Lake ice from historical records to contemporary science. *JGR Biogeosciences*, *129*(4), e2023JG007670. https://doi.org/10.1029/2023JG007670

Shinohara, R., Matsuzaki, S.-I. S., Watanabe, M., Nakagawa, M., Yoshida, H., & Kohzu, A. (2023). Heat waves can cause hypoxia in shallow lakes. *Geophysical Research Letters*, *50*(8), e2023GL102967. https://doi.org/10.1029/2023GL102967

Smith, B. J., Wagner, T. J. W., Dugan, H. A., Wilkinson, G. M., Zoet, L. K., Pujara, N., & Franck, J. A. (2025). How ice composition controls radiatively driven convection under lake ice. *Geophysical Research Letters*, *52*(19), e2025GL117454. https://doi.org/10.1029/2025GL117454

Stefan, J. (1889). Ueber die theorie der eisbildung, insbesondere über die eisbildung im polarmeere. *Annalen der Physik*, *278*(2), 269–286. https://doi.org/10.1002/andp.18912780206

SYKE. (2025). Finnish environmental institute (SYKE). Retrieved from https://www.syke.fi/fi-FI/Avoin_tieto/Ymparistotietojarjestelmat

Thiery, W., Stepanenko, V. M., Fang, X., Jöhnk, K. D., Li, Z., Martynov, A., et al. (2014). Lakemip Kivu: Evaluating the representation of a large, deep tropical lake by a set of 1-dimensional lake models. *Tellus, Ser. A*, *66*(1), 21390. https://doi.org/10.3402/tellusa.v66.21390

Toffolon, M., Cortese, L., & Bouffard, D. (2021). Self v1.0: A minimal physical model for predicting time of freeze-up in lakes. *Geoscientific Model Development*, *14*(12), 7527–7543. https://doi.org/10.5194/gmd-14-7527-2021

Toffolon, M., Piccolroaz, S., Majone, B., Soja, A.-M., Peeters, F., Schmid, M., & Wüest, A. (2014). Prediction of surface temperature in lakes with different morphology using air temperature. *Limnology & Oceanography*, *59*(6), 2185–2202. https://doi.org/10.4319/lo.2014.59.6.2185

Ventelä, A.-M., Amsinck, S. L., Kauppila, T., Johansson, L. S., Jeppesen, E., Kirkkala, T., et al. (2016). Ecosystem change in the large and shallow Lake Säkylän Pyhäjärvi, Finland, during the past 400 years: Implications for management. *Hydrobiologia*, *778*, 273–294. https://doi.org/10.1007/s10750-015-2552-2

Verpoorter, C., Kutser, T., Seekell, D., & Tranvik, L. (2014). A global inventory of lakes based on high-resolution satellite imagery. *Geophysical Research Letters*, *41*(18), 6396–6402. https://doi.org/10.1002/2014GL060641

Weyhenmeyer, G. A., Livingstone, D. M., Meili, M., Jensen, O., Benson, B., & Magnuson, J. J. (2010). Large geographical differences in the sensitivity of ice-covered lakes and rivers in the northern hemisphere to temperature changes. *Global Change Biology*, *17*(1), 268–275. https://doi.org/10.1111/j.1365-2486.2010.02249.x

Weyhenmeyer, G. A., Obertegger, U., Rudebeck, H., Jakobsson, E., Jansen, J., Zdorovennova, G., et al. (2022). Towards critical white ice conditions in lakes under global warming. *Nature Communications*, *13*(4974), 4974. https://doi.org/10.1038/s41467-022-32633-1

Woolway, R. I., Denfeld, B., Tan, Z., Jansen, J., Weyhenmeyer, G. A., & Fuente, S. L. (2021). Winter inverse lake stratification under historic and future climate change. *Limnology & Oceanography*, *7*(4), 302–311. https://doi.org/10.1002/lol2.10231

Woolway, R. I., Huang, L., Sharma, S., Lee, S.-S., Rodgers, K. B., & Timeermann, A. (2022). Lake ice will be less safe for recreation and transportation under future warming. *Earth's Future*, *10*, e2022EF002907. https://doi.org/10.1029/2022EF002907

Yang, B., Wells, M. G., McMeans, B. C., Dugan, H. A., Rusak, J. A., Weyhenmeyer, G. A., et al. (2021). A new thermal categorization of icecovered lakes. *Geophysical Research Letters*, *48*(3), e2020GL091374. https://doi.org/10.1029/2020GL091374

Yang, Y., Leppäranta, M., Cheng, B., & Li, Z. (2012). Numerical modelling of snow and ice thicknesses in lake vanajavesi, Finland. *Tellus A: Dynamic Meteorology and Oceanography*, *64*(1), 17202. https://doi.org/10.3402/tellusa.v64i0.17202

Yen, Y.-C. (1981). *Review of thermal properties of snow, ice and sea ice, Report 81-10 review*. United States Army Corps of Engineers Cold Regions Research and Engineering Laboratory Hanover.

Zhaka, V., Bridges, R., Riska, K., & Cwirzen, A. (2021). A review of level ice and brash ice growth models. *Journal of Glaciology*, *68*(270), 1–20. https://doi.org/10.1017/jog.2021.126

Zhou, X., Wang, B., Ma, X., La, Z., & Yang, K. (2024). Simulating lake ice phenology using a coupled atmosphere–lake model at Nam Co, a typical deep alpine lake on the Tibetan Plateau. *The Cryosphere*, *18*(10), 4589–4605. https://doi.org/10.5194/tc-18-4589-2024

Zhu, S., Ptak, M., Yaseen, Z. M., Dai, J., & Sivakumar, B. (2020). Forecasting surface water temperature in lakes: A comparison of approaches. *Journal of Hydrology*, *585*, 124809. https://doi.org/10.1016/j.jhydrol.2020.124809